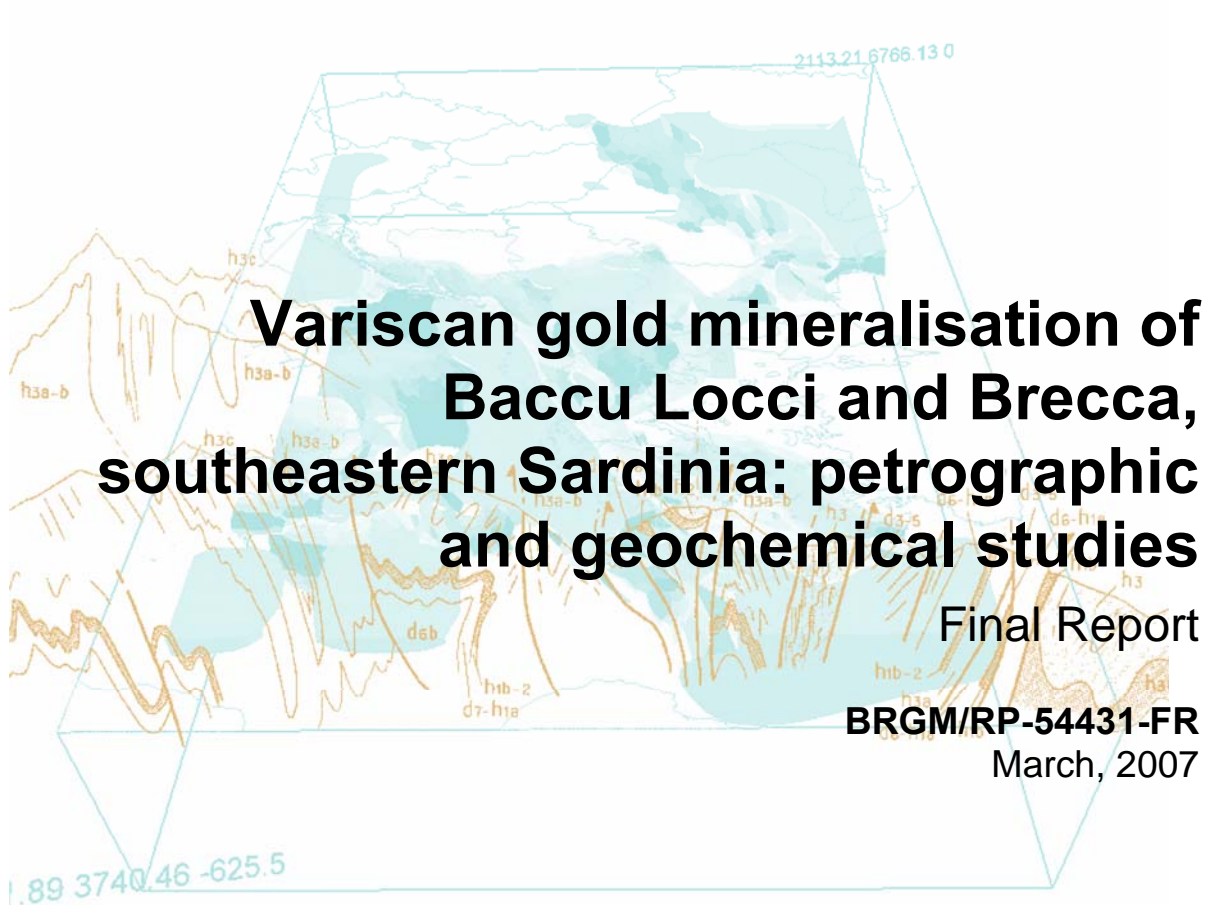


Document public





Document public

# Variscan gold mineralisation of Baccu Locci and Brecca, southeastern Sardinia: petrographic and geochemical studies

Final Report

**BRGM/RP 54431-FR**  
March, 2007

Study carried out as part of Research activities - BRGM 2006

**C. Lerouge, V. Bouchot, M. Duguet \* , S. Naitza \*\*, S. Tocco \*\* A. Funedda\*\***

With the collaboration of **J. Breton, C. Gilles**

\* University of Orléans, \*\* Cagliari University , Sardinia, Italy

<b>Checked by:</b>
Name:
Date:
Signature:
(or Original signed by:)

<b>Approved by:</b>
Name:
Date:
Signature:
(or Original signed by:)

BRGM's quality management system is certified ISO 9001:2000 by AFAQ

**Keywords:** Metallogeny, Sardinia, gold, Au-arsenopyrite, Variscan orogeny

In bibliography, this report should be cited as follows:

**C. Lerouge, V. Bouchot, M. Duguet, S. Naitza, S. Tocco, A Funedda, with the collaboration of J. Breton, C. Gilles** (2007). Variscan gold mineralisation of Baccu Locci and Brecca, southeastern Sardinia: petrographic and geochemical studies. BRGM Report N° RP-54431-FR, 20 figures, 6 tables, 47 pages, 3 annexes.

© BRGM, 2007. No part of this document may be reproduced without the prior permission of BRGM.

## Synopsis

This work was realized in the framework of the BRGM PROMET Project (PDR04-05REM03), with the collaboration, on the field in February 2004, of the Cagliari University (S. Naitza, S. Tocco, A. Funedda) and of the exploration geologists of the Sardinia Gold Mining Ltd (G.A. Farci). The purpose of this work was to characterize the Variscan gold mineralization of the Sarrabus-Gerrei region in south eastern part of Sardinia and to compare them with these of French Massif Central. In detail, two realized tasks were 1) to obtain new micro-structural constrains on the relation between black mylonites and gold mineralization of the Baccu Locci district and 2) to establish a precise paragenetic succession including Au-bearing phases of the Brecca gold mineralization.



## Contents

<b>1.</b>	<b>INTRODUCTION.....</b>	<b>9</b>
<b>2.</b>	<b>GEOLOGICAL SETTING .....</b>	<b>11</b>
2.1.	Regional Geology.....	11
2.2.	Ore deposits in SE sardinia .....	12
2.2.1.	Baccu Locci gold district.....	12
2.2.2.	Brecca gold-antimony prospect.....	17
<b>3.</b>	<b>SAMPLING .....</b>	<b>19</b>
3.1.	Baccu Locci Au district .....	19
3.2.	Brecca Au-Sb district.....	20
<b>4.</b>	<b>MINERALISED BLACK MYLONITES OF THE BACCU LOCCI AU DISTRICT .....</b>	<b>21</b>
4.1.	Stratoid mineralisation and mylonite at Su Spilloncargiu .....	21
4.2.	Black mylonite at San Riccardo .....	22
4.2.1.	sample SA 50 .....	22
4.2.2.	samples SA 53 and SA 54 .....	23
4.3.	discussion.....	26
<b>5.</b>	<b>BRECCA AU-SB MINERALIZATION.....</b>	<b>29</b>
5.1.	Sample mineralogy and textures.....	29
5.2.	Analytical techniques .....	32
5.3.	Ore characterisation .....	32
5.3.1.	sample SA8 .....	32
5.3.2.	Sample SA9 .....	34
5.3.3.	sample 11-1.....	34
5.3.4.	sample 11-2.....	35
5.3.5.	sample 11-3.....	36
5.3.6.	Sample SA19 .....	39
5.4.	conditions of ore genesis.....	40
5.4.1.	Paragenetic succession .....	40
5.4.2.	Chemical composition of arsenopyrite - Gold deposition.....	41
5.4.3.	Pressure-temperature conditions of ore deposition .....	42
<b>6.</b>	<b>DISCUSSION-CONCLUSION.....</b>	<b>43</b>
<b>7.</b>	<b>BIBLIOGRAPHY.....</b>	<b>45</b>

## List of illustrations

Figure 1 - Simplified tectonic map of Sardinia. Left: Conti et al., 1998. The small box represents the Sarrabus-Gerrei region detailed in figure 2. Right: modified after Carmignani et al., 2000, and Carmignani et al., 2001.....	10
Figure 2 - Schematic tectonic map of Sarrabus-Gerrei. SU: Sarrabus Unit; GU: Gerrei Unit; MSU: Meana Sardo unit; RGU: Riu Gruppa Unit; g: leucogranites; AF: Flumendosa Anticline; VL: Villasalto Thrust; BMZ: Baccu Locci Mylonite zone. 1. Su Suergiu Sb Mine; 2. Brecca Sb mine; 3. Baccu Locci As-Pb mine; 4. Monte Ollasteddu prospect; 5. Corti Rosas Sb mine; 6. Genna Ureu Sb-W mine. Modified after Carmignani et al., 2000.....	10
Figure 3 - A panoramic view of the old Su Spilloncargiu mine area. The old mineworks are extended for about 500 m in a NW-SE direction.....	13
Figure 4 - Textural features of the Su Spilloncargiu primary sulphide ore. Centimetric sulphide-quartz layers alternate in a dark mylonitic matrix.....	13
Figure 5 - Textural and mineralogical features of the Su Spilloncargiu (A) and San Riccardo (B, C, D) sulfide ores. Aspy: arsenopyrite, cpy: chalcopyrite, gn: galena, qtz : quartz, sph: sphalerite (from Funedda et al., 2005). .....	15
Figure 6 - Geological sketch map of the Baccu Locci district (after Conti et al., 1998). S: Su Spilloncargiu mineworks; SR: San Riccardo mineworks. ....	16
Figure 7 - photos of the outcrops. A,C - auriferous quartz vein of San Riccardo; B, D - black mylonite of the footwall of the auriferous vein of San Riccardo; E - overview of the Brecca prospect hosted by Ordovician porphyritic intrusive; F – stibnite-bearing vein of Brecca. The two samples of Su Spilloncargiu, SA 31 and SA 32, were collected from the stratoid mineralisation.....	19
Figure 8 - micrographs of Baccu Locci mylonite zone – Su Spilloncargiu (SA 31). ....	21
Figure 9 - Micrographs of San Riccardo mylonite zone, sample 52. A – quartz lens deformed in a shear band (LN). B- microlithons of sericite and associated crenulation (LP). C- arsenopyrite and feldspar brechified by veinlets of quartz (LP). D- same thing but in reflected light. E- brechified arsenopyrite replaced by galena and chalcopyrite. FK = Kfeldspar, Ap = arsenopyrite, Ga = galena, Cp = chalcopyrite, Q2 = secondary veinlet of microcrystalline quartz. ....	24
Figure 10 - micrographs of Baccu Locci mylonite zone – San Riccardo vein, sample 53. A – strain-slip showing microlithons with metamorphic muscovite that is partially hydrothermalized. B – Tension gashes with senestral quartz (LN). C- ductile shear bands affecting quartz veins. D – late veins with muscovite. These veinlets crosscut the microfaults infilled with organic matter. E – brittle-ductile shear bands reworking mylonitic fabric. Mu = muscovite, Se = sericite. ....	25
Figure 11 - micrographs of Brecca mineralization – microtextures of the sample SA8 .....	27
Figure 12 - micrographs of Brecca mineralization – samples SA9 and SA11-1 .....	30
Figure 13 - micrographs of Brecca mineralization – microtextures of the samples SA11-2 and SA11-3.....	31



Figure 14 - SEM backscattered electron image of ore in sample SA8 .....	33
Figure 15 - SEM backscattered electron image of ore in sample SA9 .....	34
Figure 17 - Backscattered electron image of arsenopyrite in sample 11-2. ....	35
Figure 18 - SEM backscattered electron image of ore in sample SA11-3.....	37
Figure 19 - Element cartography of two zoned grains of arsenopyrite – The euhedral grains of arsenopyrite show a chemical zoning with a core enriched in S and Sb and a rim enriched in As. Small inclusions of gold are observed in the core of arsenopyrite grains.....	38
Figure 20 - micrographs of sample SA19. a. weathered arsenopyrite; b., c. particles of gold in weathered arsenopyrite .....	39

## List of tables

Table 1 - Paragenetic succession of the Su Spilloncargiu deposit, deduced from the mineralogical observations of previous works (Zucchetti, 1958; Bakos et al., 1991; Funedda et al., 2005) (cf illustrations in Figure 5A ) .....	14
Table 2 - Paragenetic succession of the San Riccardo deposit, deduced from the mineralogical observations of previous works (Zucchetti, 1958; Bakos et al., 1991; Funedda et al., 2005) (cf illustrations in Figure 5 B to D). ....	14
Table 3 - detection limits of elements analyzed in arsenopyrite, taking account analytical conditions. ....	32
Table 4 - description of the major stages of ore deposition observed in the five studied samples of ore from the Brecca ore deposit .....	40
Table 5 - Summary of the chemical variations of arsenopyrite related with its type and with its zoning.....	41
Table 6 - description of the major stages observed in the five studied samples of ore from the Brecca ore deposit.....	41

## List of appendices

Annexe 1 - whole-rock geochemical data of the Spilloncargiu and San Riccardo ore deposits.....	47
Annexe 2 - EPMA analyses of arsenopyrite from the Brecca Au-Sb ore deposit.....	51
Annexe 3– EPMA analyses of tetrahedrite from the Brecca Au-Sb ore deposit.....	55



# 1. Introduction

This work was realized in the framework of the BRGM PROMET scientific project (PDR04-05REM03), with the collaboration, on the field in February 2004, of the Cagliari University (S. Naitza, S. Tocco, A. Funedda) and of the exploration geologists of the Sardinia Gold Mining Ltd (G.A. Farci).

This study has two main tasks :

1) petrographic characterization of the "black mylonites" (named following macroscopic description) that are sometimes found to be spatially associated with the gold-bearing Variscan deposits of the Sardinian gold district. For this purpose, two sites in the Baccu Locci prospect were selected: Su Spilloncargiu and San Riccardo. The approach consisted of a petrostructural analysis of five rock samples (orientated polished thin sections), to study the relationship between the deformation and the hydrothermal processes observed.

2) Textural and chemical characterization of the mineralization from the Au-Sb Brecca prospect. The approach consisted of a microtextural and chemical analysis of seven rock samples (polished thin sections) in order to determine a paragenetic succession and to locate gold in this succession.

Finally, results were compared with previous works on Variscan gold mineralization in the Variscan belt of Europe.

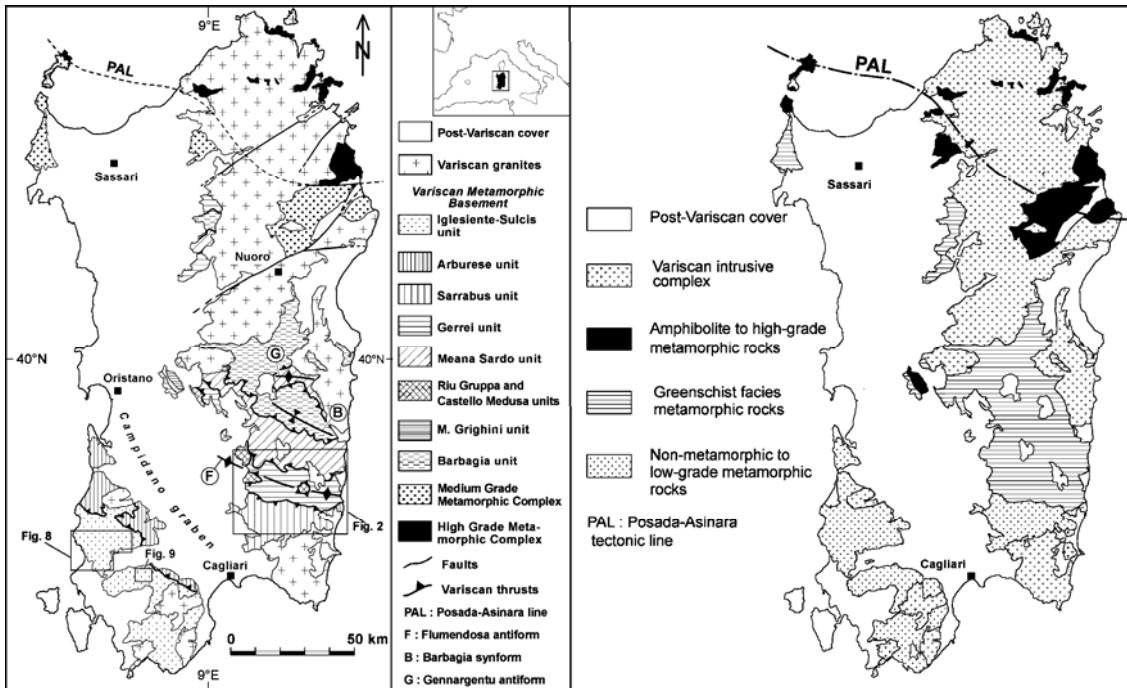


Figure 1 - Simplified tectonic map of Sardinia. Left: Conti et al., 1998. The small box represents the Sarrabus-Gerrei region detailed in figure 2. Right: modified after Carmignani et al., 2000, and Carmignani et al., 2001.

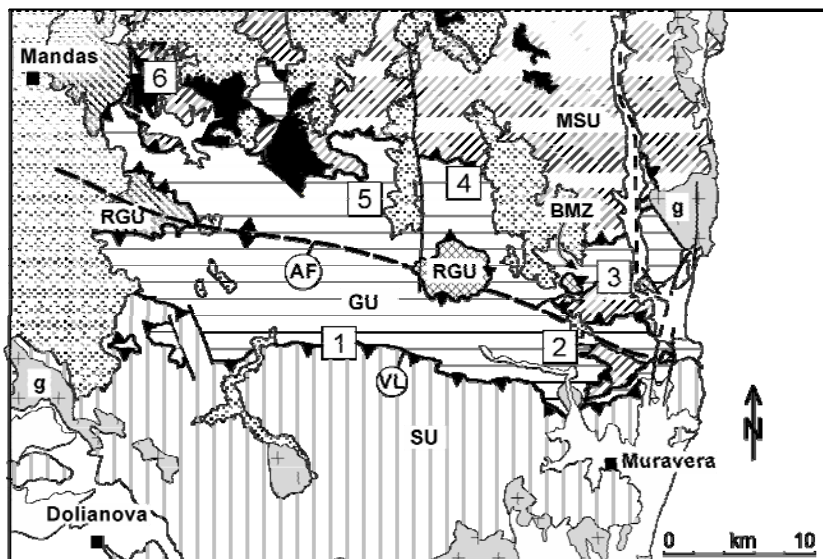


Figure 2 - Schematic tectonic map of Sarrabus-Gerrei. SU: Sarrabus Unit; GU: Gerrei Unit; MSU: Meana Sardo unit; RGU: Riu Gruppa Unit; g: leucogranites; AF: Flumendosa Anticline; VL: Villasalto Thrust; BMZ: Baccu Locci Mylonite zone. 1. Su Suergiu Sb Mine; 2. Brecca Sb mine; 3. Baccu Locci As-Pb mine; 4. Monte Ollasteddu prospect; 5. Corti Rosas Sb mine; 6. Genna Ureu Sb-W mine. Modified after Carmignani et al., 2000.

## 2. Geological setting

### 2.1. REGIONAL GEOLOGY

Most of Sardinia is underlain by Paleozoic (Cambrian-Carboniferous) volcano-sedimentary successions, deformed during the Hercynian Orogeny between 360 and 300 Ma (Figure 1). In the southeastern part of Sardinia, the authors recognise several tectonic phases:

- D1: a first compressional phase corresponding to tangential tectonics with a southern vergence, responsible for the formation of overturned recumbent folds in the south and for stacking. Then, we can identify, from north to south and from top to bottom, the Barbagia, Meana Sardo, Gerrei and Riu Gruppa units. This deformation phase took place under epizonal metamorphic conditions. The boundary between the tectonic units is outlined by mylonitic shear zones up to 2-300 meters in thickness.
- D2: a second compressional deformation phase showing a westward vergence, restricted to the southern part of Sardinia where a new unit (Sarrabus) overthrusts to the west the Riu Gruppa and Gerrei units. Evidence of this westward thrusting also exists in the southwestern part of Sardinia. Metamorphism is very weak and never exceeds anchizonal conditions.
- D3: a last compressional phase affecting the stacked nappe column, reflected by upright folds trending NW-SE that refolded the successions into broad synforms and antiforms several kilometres wide (NE-SW shortening). A good example is the Flumendosa antiform, rich in Au Sb and/or W-bearing mineralisation of orogenic origin.
- A late extensional phase, contemporaneous with widespread collapse of the mountain range, has been described in this region. This post-orogenic phase is thought to have occurred around 300 Ma and is reflected by reactivation of the early thrusts with a ductile-brittle normal displacement. These shallow-dipping normal faults are associated with collapsed folds with NW-SE axes and variable vergence. Note that these normal faults are also present on the limbs of D3 antiforms with opposing displacement on either side of the fold hinges. This tectonic activity was associated with the widespread emplacement of granitic suites, the largest being located in northeastern Sardinia.

During the Permian, a few sedimentary basins (red pelite) associated with erosion of the range are affected by rhyolitic extrusion. Tertiary (30-19 Ma) arc and back-arc successions also crop out abundantly in Sardinia. They are the result of the opening of a back-arc basin in the Gulf of Lions in relation to westward-dipping subduction

beneath Sardinia. These volcanic rocks host gold epithermal-type mineralisation that is mined at Furtei.

## **2.2. ORE DEPOSITS IN SE SARDINIA**

### **2.2.1. Baccu Locci gold district**

The Baccu Locci mineralization occurs as stratabound bodies (Su Spilloncargiu deposit) and discordant veins (San Ricardo deposit) confined to the Ordovician-Silurian volcano-sedimentary sequence of SE Sardinia (Figure 2). The mineral association is given by As-Fe-Cu-Pb-Zn sulfides and sulfosalts with minor gold-electrum. According to Bakos et al. (1991), it results of a complex evolution starting with the Silurian submarine volcanic activity through different mobilization and concentration processes related to the Variscan tectono-metamorphic-magmatic event.

The deposits of Baccu Locci district (Eastern Gerrei) were mined for As and Pb minerals during the 20th century (Garbarino et al., 2003). We distinguish two main types of mineralisation:

- A stratoid-type, because it shows horizontal bedding of indeterminate origin (sedimentary or tectonic bedding?), is well described in Su Spilloncargiu deposit (Figure 3, Figure 4). This stratabound mineralisation has been interpreted in several ways by different Authors: 1) volcano-sedimentary (Schneider, 1972; Bakos et al., 1991), 2) metamorphogenic, due to a mylonitisation of Silurian black shales (Conti et al., 1998) and 3) hydrothermal (Zucchetti, 1958; Garbarino et al., 2003; Funedda et al., 2005). Stratabound ores are located just below an ancient paleosurface and covered by Eocene marine sediments. The mineralisation consists of siliceous impregnations containing galena, chalcopyrite, sphalerite, arsenopyrite, and (gold-free) arsenates, with local lenses of massive sulphides, particularly sphalerite and galena (Table 1, Figure 5-A, Annexe 1). Secondary sulphides and oxidates, related to supergen process, are particularly abundant (Table 1). The mineralisation could be rich in carbonaceous material;
- A discordant type, well described in San Riccardo deposit, corresponding to steeply dipping quartz veins with subordinate sulphides, namely arsenopyrite, base metal sulfides (Pb-Zn-Cu-Sb) and trace of gold-electrum (samples with up to 6 g/t Au) (Table 2, Figure 5-B to D, Annexe 1).

Although somewhat problematic, the spatial relationships between these two types of mineralisation are quite evident at the outcrop scale, with the discordant subvertical veins apparently cross-cutting the stratabound mineralisation (Funedda et al., 2005). Bakos et al. (1991) interpreted these mineralizations as derived from a multistage mineralizing process, with the setting of quartz-arsenopyrite veins in the later stages suggesting remobilization process. Recent structural studies (Conti et al. 1998) suggest the Baccu Locci district is included by the NW-SE trending Baccu Locci

Mylonitic Zone (Figure 6), the most important km-scale shear zone in Northern Gerrei. In the same way, according to Garbarino et al. (2003), the orebodies are hosted in strongly tectonized lithologies as mylonitized metasiltstones and metarhyolites. They interpreted in particular the Baccu Locci lenticular ores (Su Spilloncargiu) as spatially related to the mylonitic fabric. New information concerning the formation of supposed mylonites will be discussed later, based on new microtextural studies.



Figure 3 - A panoramic view of the old Su Spilloncargiu mine area. The old mineworks are extended for about 500 m in a NW-SE direction.

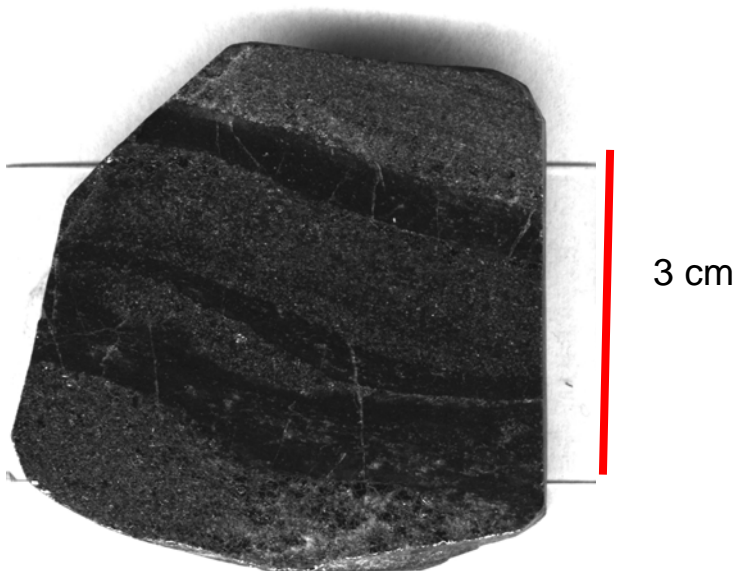


Figure 4 - Textural features of the Su Spilloncargiu primary sulphide ore. Centimetric sulphide-quartz layers alternate in a dark mylonitic matrix.

Table 1 - Paragenetic succession of the Su Spilloncargiu deposit, deduced from the mineralogical observations of previous works (Zucchetti, 1958; Bakos et al., 1991; Funedda et al., 2005) (cf illustrations in Figure 5A )

		Zn-Fe stage	Pb-Cu-As-Zn stage	supergenic alteration stage
sphalerite	Zn S	-----	----	
pyrrhothite	Fe <sub>1-x</sub> S	---		
galena	PbS		-----	-----
chalcopryrite	CuFeS <sub>2</sub>		-----	
arsenopyrite	FeAsS		----	
falhore	(Cu,Ag,Fe,Zn) <sub>12</sub> (Sb,As) <sub>4</sub> S <sub>13</sub>		---	
pyrite	FeS <sub>2</sub>	---		-----
bornite	Cu <sub>5</sub> FeS <sub>4</sub>			-----
covellite	CuS			-----
chalcocite	Cu <sub>2</sub> S			-----
native copper	Cu			---
cuprite	Cu <sub>2</sub> O			-----
malachite	Cu <sub>2</sub> (CO <sub>3</sub> ) <sub>2</sub> (OH) <sub>2</sub>			-----
azurite	Cu <sub>3</sub> (CO <sub>3</sub> ) <sub>2</sub> (OH) <sub>2</sub>			-----

Table 2 - Paragenetic succession of the San Riccardo deposit, deduced from the mineralogical observations of previous works (Zucchetti, 1958; Bakos et al., 1991; Funedda et al., 2005) (cf illustrations in Figure 5 B to D).

		As-Fe stage	Pb-Cu-Zn stage	Sb- Ag -Au stage	supergenic alteration stage
Arsenopyrite	FeAsS	-----	-----		
Pyrite	FeS <sub>2</sub>	-----	---?		-----
galena	PbS		-----		
Chalcopryrite	CuFeS <sub>2</sub>		-----		
Sphalerite	Zn S	--?	-----		
pyrrhothite	Fe <sub>1-x</sub> S	--?			
Falhore				-----	
Stibnite				--	
gold/electrum	(Ag, Au)			-----	
Bornite	Cu <sub>5</sub> FeS <sub>4</sub>				-----
Covellite	CuS				-----



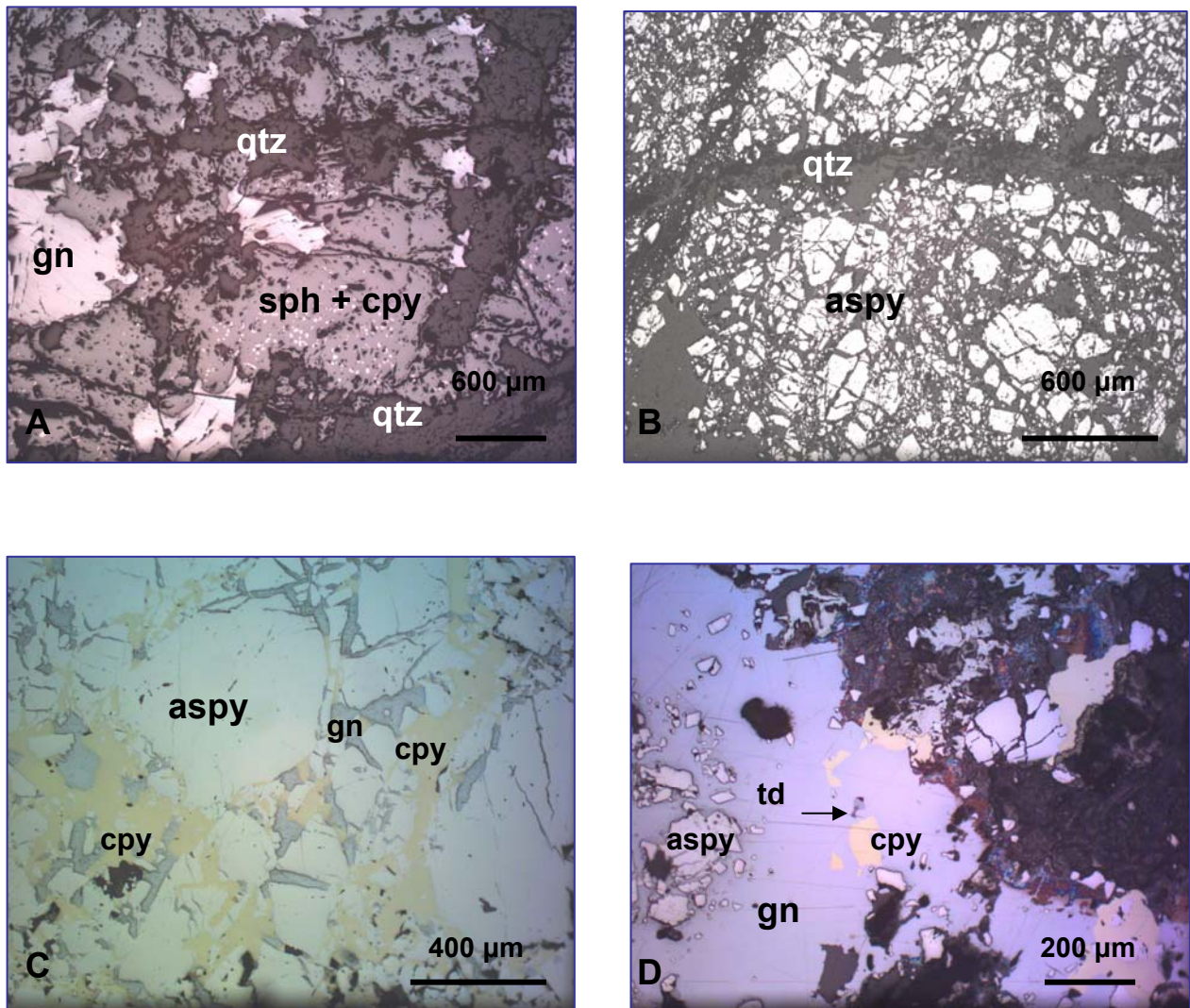


Figure 5 - Textural and mineralogical features of the Su Spilloncargiu (A) and San Riccardo (B, C, D) sulfide ores. Aspy: arsenopyrite, cpy: chalcopyrite, gn: galena, qtz : quartz, sph: sphalerite (from Funedda et al., 2005).

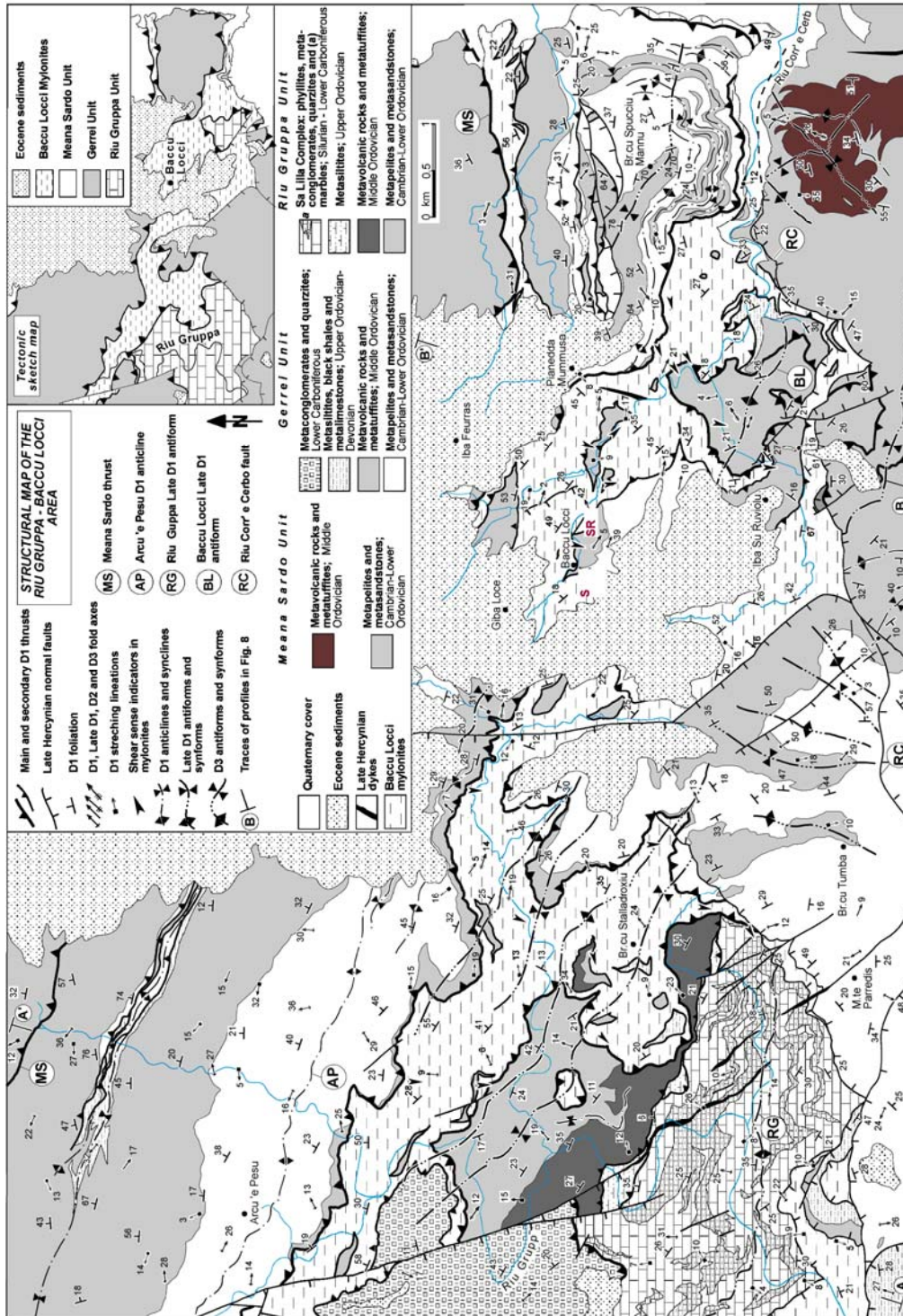


Figure 6 - Geological sketch map of the Baccu Locci district (after Conti et al., 1998). S: Su Spilloncargiu mineworks; SR: San Riccardo mineworks.

### 2.2.2. Brecca gold-antimony prospect

Mineralisation of the Au-Sb Brecca prospect is hosted by Ordovician porphyritic acidic metavolcanites and controlled by sub-E-W (N 100°E to N 60-80°E) trending structures, with a dip of 45° northward. During Early Carboniferous, porphyritic rhyolite have been affected by a weakly developed regional schistosity (S1) following by a NW-SE trending folding (D3) associated with a crenulation cleavage (S3: 140 E 45).

Two main types of mineralisation are observed :

- gold type (high tonnage low grade mineralization) : Network of cm- to dm-thick veinlets and lenses of grey microcrystalline quartz with disseminated fine-grained pyrite and arsenopyrite which exhibit gold grades of 1.21 g/t on 21 meters. Native gold was very rarely observed. Hydrothermalized porphyritic facies with only disseminated fine-grained sulfides can be observed as well.
- antimony type: Stibnite bearing veinlets and veins crosscutting hydrothermalized facies. A 80°N trending and 45°S dipping vein have been exploited. Its geometry suggest a sinistral-reverse movement according to a possible N 60°E trending shortening.



## 3. Sampling

### 3.1. BACCU LOCCI AU DISTRICT

Five samples from the Baccu Locci district were collected on two outcrops: two from Su Spilloncargiu and three from San Riccardo (Figure 7, A to D).

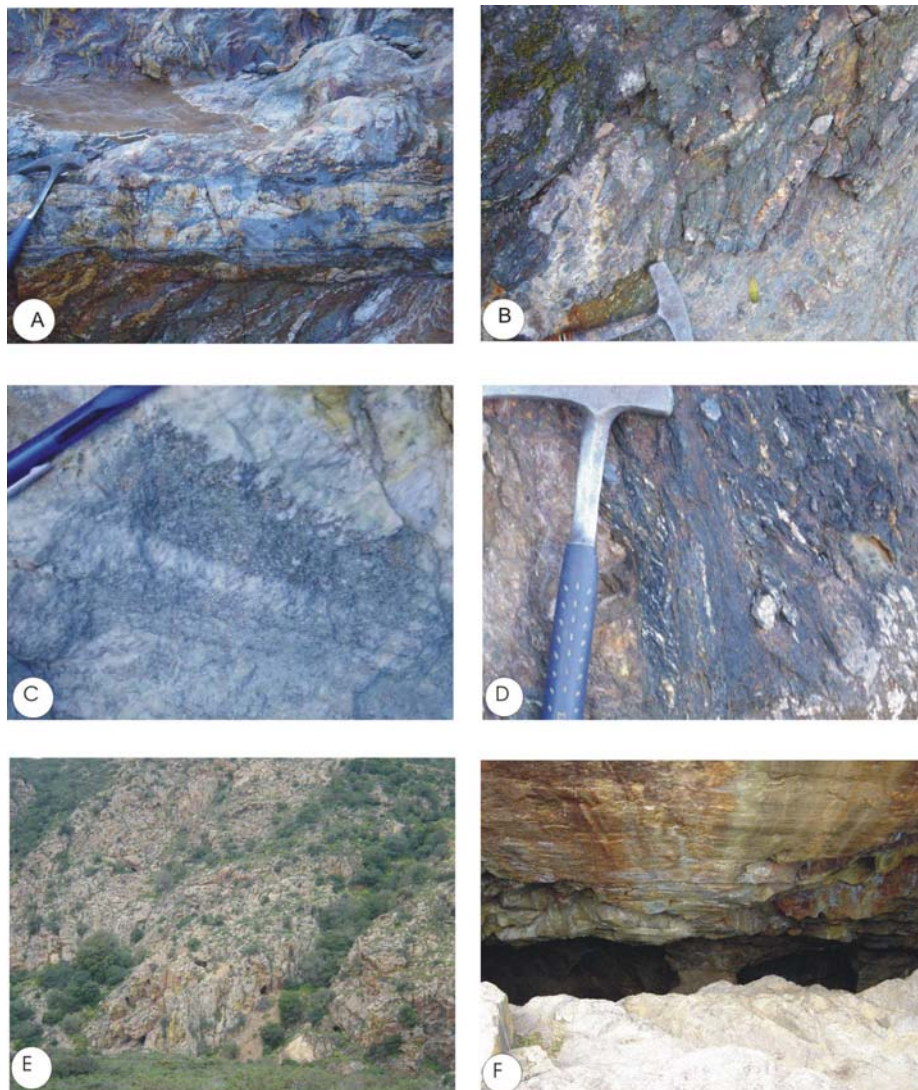


Figure 7 - photos of the outcrops. A,C - auriferous quartz vein of San Riccardo; B, D - black mylonite of the footwall of the auriferous vein of San Riccardo; E - overview of the Brecca prospect hosted by Ordovician porphyritic intrusive; F - stibnite-bearing vein of Brecca. The two samples of Su Spilloncargiu, SA 31 and SA 32, were collected from the stratoid mineralisation.

The three samples of San Riccardo, SA 50, 53, and 54 were collected from mylonites located in the overlying and wall rocks of the San Riccardo gold-bearing veins.

Our macroscopic field observations in San Riccardo show that:

- the N130°E- trending, 60° SW dipping gold bearing vein is hosted in black cataclastic/mylonitic shale interpreted as “black mylonite” sub-parallel to the vein. This cataclastic/mylonitic narrow zone cuts the regional schistosity S1 and Baccu Locci mylonite.
- structural criteria (tension gashes, drag fold, S/C plans) in the mylonite suggest a gold bearing quartz vein emplacement along a strike slip cataclastic/mylonitic zone, with a mainly dextral movement.
- emplacement of a lamprophyre dyke sub-parallel to the gold-bearing veins seems later than the mineralisation. The relative chronology is as follows: 1) black mylonite, 2) Au vein, 3) lamprophyre.

### **3.2. BRECCA AU-SB DISTRICT**

In the Brecca zone Ordovician metamorphosed “porphyritic” volcanic and epiclastic rocks shows N100°E and N60-80°E 45N faults (Figure 7E). Au-Sb mineralization consists of:

- 1) disseminated sulfides in hydrothermalized “porphyritic” volcanic rocks;
- 2) network of veinlets and centimeter-sized lenses of grey jaspoid quartz with fine-grained disseminated sulfides (pyrite and arsenopyrite) which exhibit significant gold content (21 m with 1.21 g/t);
- 3) veinlets of stibnite crosscutting hydrothermalized facies.

Six samples representative of the mineralization were collected: SA8, SA9, SA11-1, SA11-2, SA11-3, SA19.

## 4. Mineralised black mylonites of the Baccu Locci Au district

### 4.1. STRATOID MINERALISATION AND MYLONITE AT SU SPILLONCARGIU

Samples SA 31 and SA 32 were collected from the stratabound mineralisation. They are essentially composed of microcrystalline quartz with no particular fabric (Figure 8A). The only orientation identified in thin section is suggested by veinlets of an amorphous material (organic matter?) parallel to the fabric observed at macroscopic scale. It is difficult to establish the nature of this inherited fabric (schistosity or sedimentary bedding?). Carbonate veins occasionally follow these structures (Figure 8B). In contrast to the siliceous matrix, which is free of mineralisation, these black veinlets occasionally contain sulphides (Figure 8C). These structures sometimes cut the principal fabric, where they seem to form stylolitic structures and tension cracks (Figure 8D).

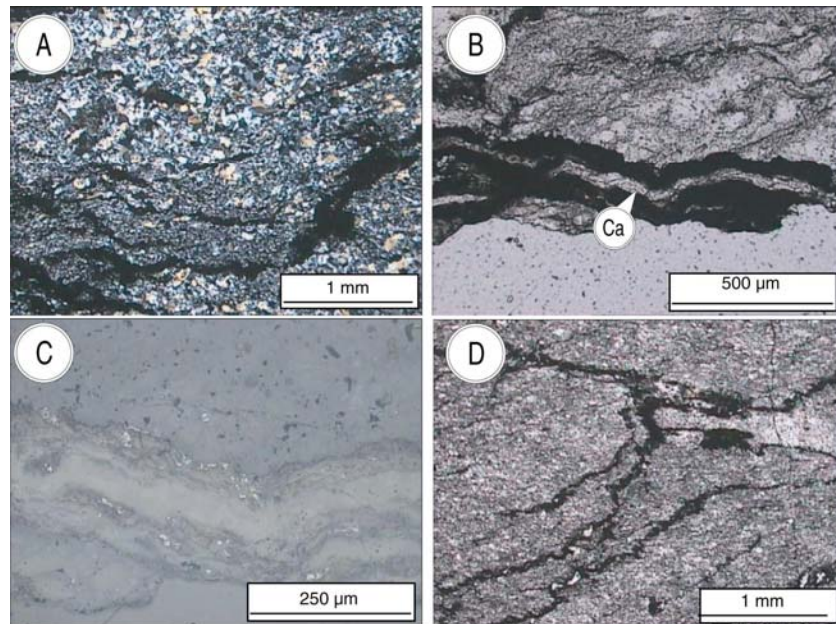


Figure 8 - micrographs of Baccu Locci mylonite zone – Su Spilloncargiu (SA 31).

*Legend: A – This sample is essentially composed of microcrystalline quartz without any fabric. The only fabric is underlined by black material (LP). B – detail of planar structures that contain carbonates veinlets (reflected light). C- Rare mineralisation associated with planar structures. D – black planar structures that are sometimes connected. It could be stylolitic structures associated with slices and opening parallel to a bedding. Ca = carbonate.*

The siliceous facies suggests a massive silicification of a material of undetermined origin. However, it is unlikely to have been the black Silurian shale, as some authors suggest. In fact, the country rock is mainly composed of Ordovician porphyritic rocks. The silica impregnation, possibly related to supergen process, is sufficiently intense that the presence of an earlier mylonitic fabric cannot *a priori* be excluded.

## 4.2. BLACK MYLONITE AT SAN RICCARDO

Samples SA 50, 53, and 54 were collected from mylonites located in the overlying and wall rocks of the San Riccardo gold-bearing quartz veins.

### 4.2.1. sample SA 50

In contrast to the samples from Su Spilloncargiu (SA 31-32), these samples show a well-developed foliation. The matrix consists of an alternation of sericitic felting and a dark amorphous material that is much more abundant than in samples SA31-32. This matrix surrounds boudinaged quartz and less commonly feldspar phenocrysts, elongated parallel to the foliation (Figure 9A). Some of these quartz phenocrysts show discontinuous plastic deformation of the quartz, with wavy extinction and the presence of prismatic sub-boundaries that indicate the action of a basal <a> intra-crystalline slip system (required temperature of about 350°C). The sericitic matrix is highly deformed, with shear bands and a crenulation schistosity parallel to the principal schistosity observed in the field (Figure 9B). Bands of late, ductile-brittle shearing cut the quartz boudins.

Two mineralising events were identified in samples collected in the cataclastic zone:

- **The first (arsenopyrite) event** is associated with boudins of coarse- to fine-grained quartz and feldspar during late brittle –ductile shearing (Figure 9C); it could be related to the emplacement of the closed gold-bearing quartz vein ore containing amount of early arsenopyrite;
- **The second (chalcopyrite + galena) event** is associated with microcrystalline quartz veinlets that cut the quartz boudins and the early arsenopyrite, but not the sericitic matrix (Figure 9C, D, and E). This event could be related to the paragenesis containing base metal sulfides (galena-chalcopyrite-sphalerite) and trace of gold-electrum, later in the arsenopyrite bearing quartz vein.

Based on these observations, we can propose the following sequence:

- 1- After the regional mylonitisation (Baccu Locci mylonite, Conti et al, 1998), hydrothermal activity affects the protolith and produces massive sericitisation of the rock as well as the formation of lenses ("boudins") and veinlets of quartz and arsenopyrite, parallel to the principal mylonitic fabric.
- 2- Emplacement of quartz veinlets with chalcopyrite and galena. These veinlets cut the earlier fabric.



**3-** Deformation continues and preferentially affects the sericitic layers. The stage-2 quartz veinlets in the matrix are thereby destroyed. A crenulation schistosity seems to be contemporaneous with this event.

**4-** Last stage of hydrothermal activity, with emplacement of veinlets of sericite and dark material that cut across the earlier structures. These veinlets occasionally follow the existing structures. This event takes place during a ductile-brittle deformation expressed by the presence of shear bands that cross-cut the earlier structures.

These observations show that both hydrothermal episodes are contemporaneous with the ductile-brittle shearing of these rocks. The deformation continued after these two hydrothermal episodes, since the quartz veinlets from the second episode are not found in the matrix. The same is true for the hydrothermal activity, which continued after the first two episodes, as shown by the veinlets of sericite and extremely abundant dark material that cut all the structures described above.

This sequence of hydrothermal events is similar to that known, for example, in the Bourneix orogenic gold deposits (Bouchot et al., 1990), in the French Massif Central.

However, the timing of the emplacement of what has been referred to as "dark mylonite" remains unclear. Although, as previously noted, some of the structures involving the dark material are related to the regional mylonitisation, there is some reason to think that, at least, part of it may be related to the hydrothermal activity.

#### **4.2.2. samples SA 53 and SA 54**

Examination of these samples will enable the kinematics of the various tectonic events to be defined. Although these samples are less affected by hydrothermal activity than SA 50, they nevertheless show traces of significant alteration (leaching?, Figure 10A). An early dextral sense of movement was identified, in particular by the presence of shear bands and the asymmetrical appearance of the quartz boudins. This mylonitic fabric is in turn affected by quartz- and feldspar-filled, asymmetrical tension cracks that give a sinistral shear direction (Figure 10B). Sericite veinlets, which may be contemporaneous with these tension cracks and quartz veinlets, have also been described (Figure 10D). These samples also show conjugate ductile-brittle shear bands giving sense of movement of the shearing that are sometimes dextral, sometimes sinistral, and that cut all the structures described previously (Figure 10C and D). The protolith seems to represent a volcano-sedimentary facies, though not a "porphyritic rock" as strictly defined. This facies includes an alternation of pelitic beds with large white mica flakes elongated parallel to the foliation, and more clastic quartzo-feldspathic beds. These observations show that the protolith had already been metamorphosed (regional metamorphism) prior to being altered during the hydrothermal event.

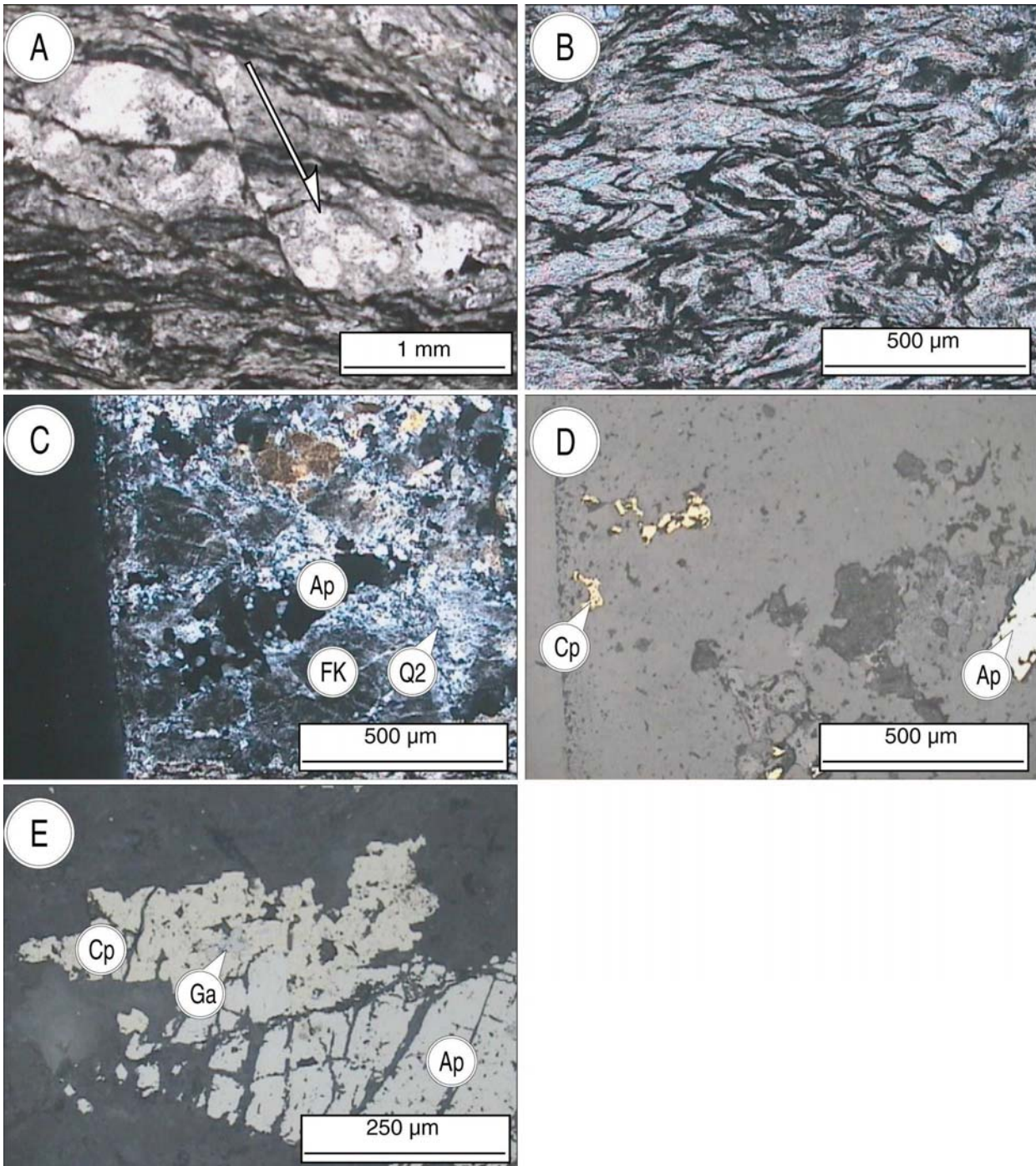


Figure 9 - Micrographs of San Riccardo mylonite zone, sample 52. A – quartz lens deformed in a shear band (LN). B- microlithons of sericite and associated crenulation (LP). C- arsenopyrite and feldspar brechified by veinlets of quartz (LP). D- same thing but in reflected light. E- brechified arsenopyrite replaced by galena and chalcopyrite. FK = Kfeldspar, Ap = arsenopyrite, Ga = galena, Cp = chalcopyrite, Q2 = secondary veinlet of microcrystalline quartz.

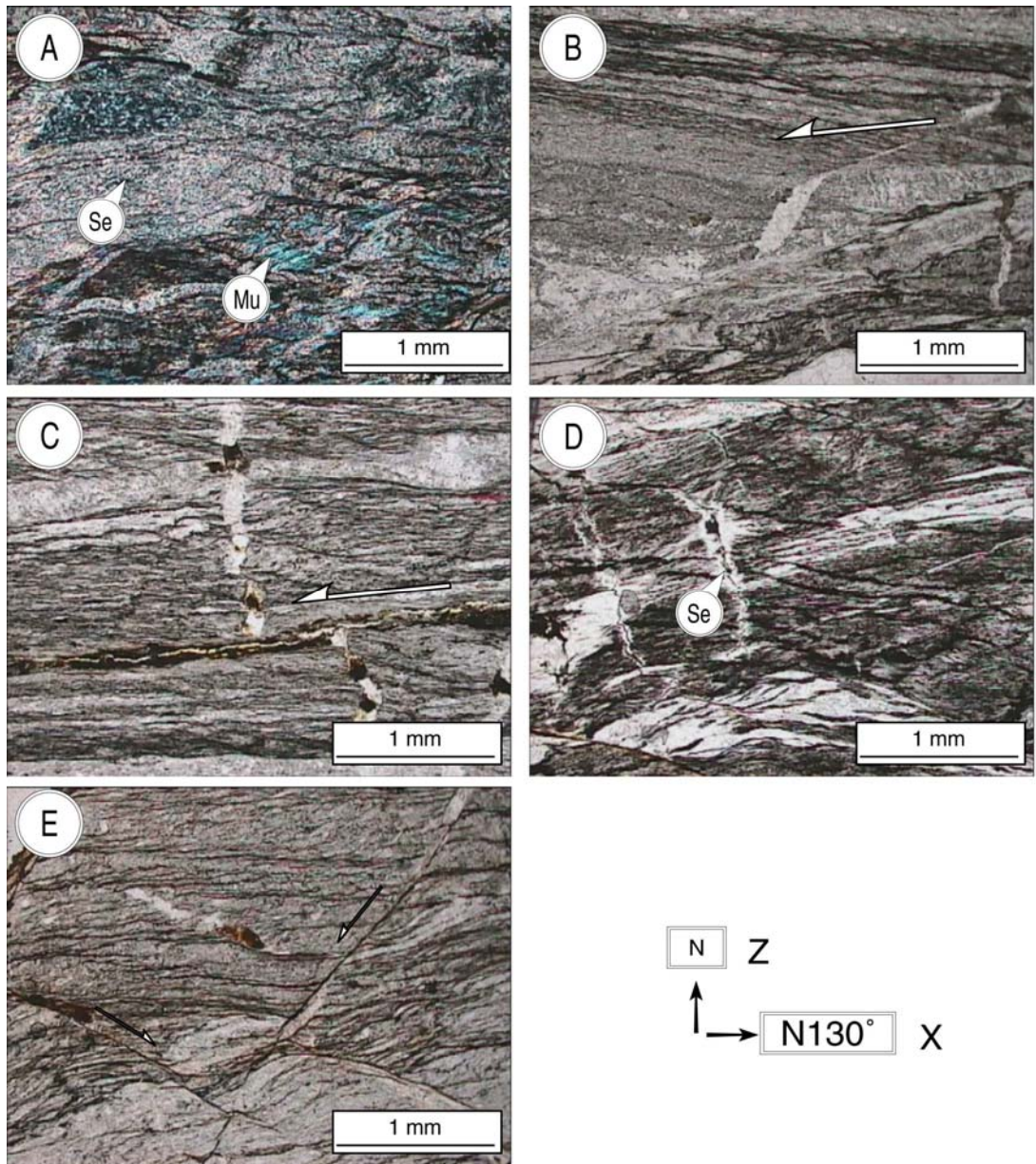


Figure 10 - micrographs of Baccu Locci mylonite zone – San Riccardo vein, sample 53. A – strain-slip showing microlithons with metamorphic muscovite that is partially hydrothermalized. B – Tension gashes with senestral quartz (LN). C- ductile shear bands affecting quartz veins. D – late veins with muscovite. These veinlets crosscut the microfaults infilled with organic matter. E – brittle-ductile shear bands reworking mylonitic fabric. Mu = muscovite, Se = sericite.

### 4.3. DISCUSSION

This study once again underlines the close relationship that exists between deformation and hydrothermal activity in the gold districts. At San Riccardo (sample SA 50), the deformation is very intense, polyphase, and shows diminishing intensity. In fact, a completely ductile deformation (regional) changes progressively into a deformation that is ductile-brittle to brittle. This deformation is accompanied by a hydrothermal activity that also decreases in intensity, along with the deformation. Because of its nature (quartz veins, potassic alteration), the hydrothermal activity seems to control the rheology of the materials and hence their mode of deformation. Thus, during a potassic alteration, the sericitic matrix will absorb most of the non-coaxial deformation. The deformation will then be thoroughly ductile in nature. The term "black mylonite" is thus perfectly appropriate for San Riccardo, since these rocks have undergone ductile deformation. In the case of sample SA 53, the protolith seems to have been a metapelite. It does not appear different from other black mylonites described in similar environments like the French Massif Central (Bourneix gold deposit, Bouchot et al., 1990) and beyond (Ashanti gold deposit in Ghana, Allibone, 2002). As regards Su Spilloncargiu, the silicification is so strong that any trace of deformation - if indeed there was any - has disappeared.

An important question that has not yet been resolved concerns the nature of the so-called dark material, which is present in large quantities in all the samples. In the SA 53 samples it seems to appear at several stages in the deformation history. It is very frequently associated with the preferred plane of deformation (plane of schistosity, foliation, microfaulting) and seems to be of various types (oxides and/or organic matter).

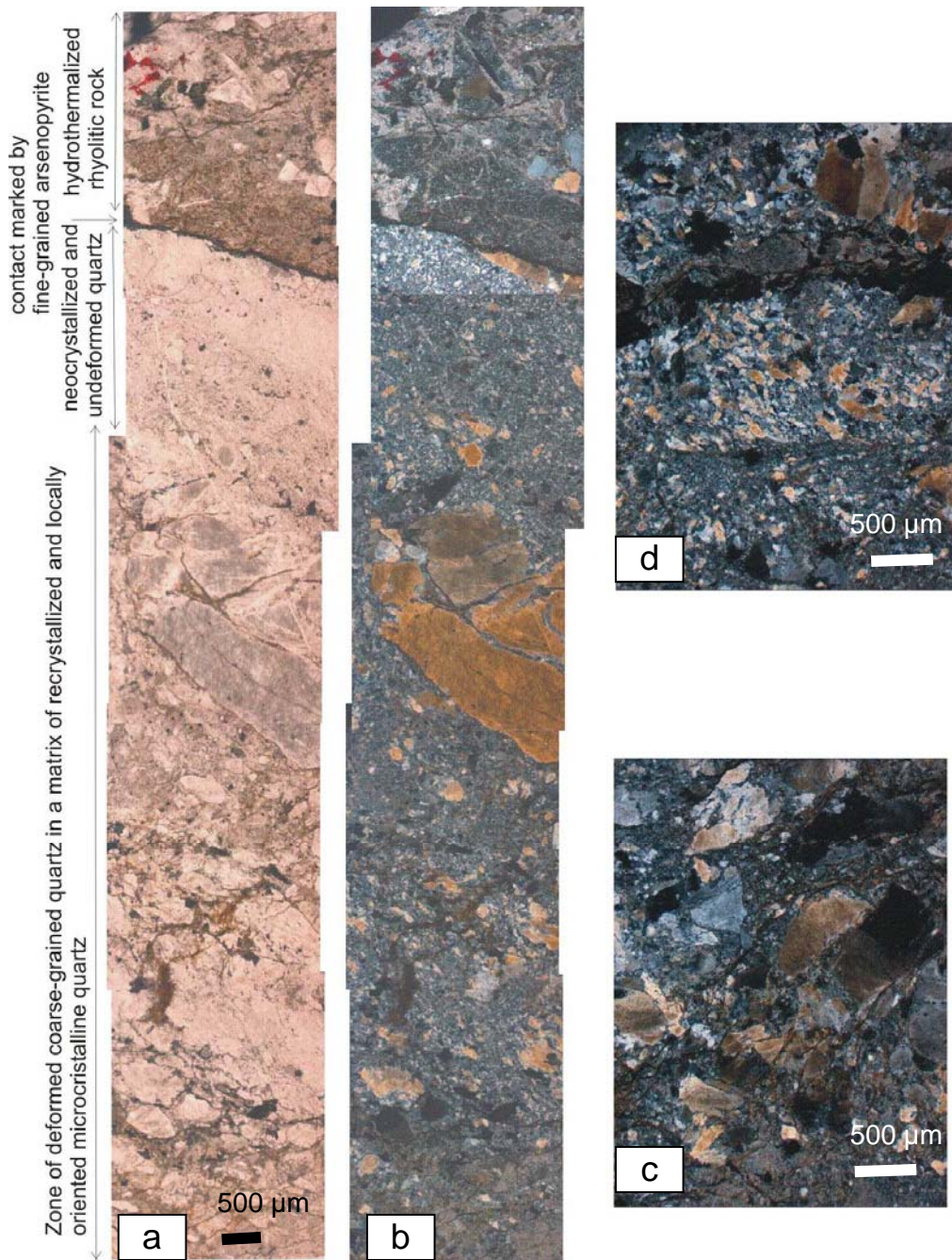


Figure 11 - micrographs of Brecca mineralization – microtextures of the sample SA8

*a (LN), b (LP). overview of the texture of the quartz vein in contact with the hydrothermalized host rock. c. detail of a relictual deformed coarse-grained quartz which shows partial recrystallizations at its rims in contact with a matrix of microcrystalline quartz. d. microcrystalline quartz showing a fabric oblique on the general trending marked by the contact, by elongated elements of hydrothermalized hostrock and by late veinlets of fine-grained arsenopyrite.*



## 5. Brecca Au-Sb mineralization

### 5.1. SAMPLE MINERALOGY AND TEXTURES

**SA8** is a highly hydrothermalized and deformed rhyolitic/rhyodacitic pyroclastic rock. The direction of shearing is underlined by a zone of deformed and relatively aligned grey coarse-grained quartz and elements of rhyolitic rock in a matrix of recrystallized quartz grains showing locally a fabric (Figure 11). At the contact between this deformed zone and hydrothermalized rhyolitic rock, a ribbon of relative undeformed and elongated quartz grains neocrystallized, probably late to the deformation phase. Rhyolitic rock contains quartz phenocrysts in a matrix of quartz and white mica; the whole rock is brecciated associated with an infilling of white mica. Mineralization occurs as early scarce disseminated arsenopyrite and pyrite preferentially associated with white mica in relics of hydrothermalized rhyolitic rock, and as very fine veinlets of arsenopyrite along grain boundaries and deformation microstructures in the deformed part. Most of the arsenopyrite is highly transformed in scorodite, specially the second generation. This sample was collected in the 21 meters - thick zone with a gold grade of 8-9 g/t. Gold is not visible.

**SA9** is a wholly hydrothermalized rhyolite or crystal-bearing tuf/tuffite containing preserved phenocrysts quartz and large flakes of white mica with numerous titanium oxides which could be primary biotite (Figure 12). The hydrothermal alteration is characterized by a crystallization of quartz, white mica (sericite), and rare feldspar in the matrix. The rock shows a slight deformation marked by the recrystallization of quartz-eyes in medium-grained quartz. Sulfides occurs as arsenopyrite, stibnite and sphalerite. Arsenopyrite is rare and occurs as disseminated automorphic grains. Stibnite is abundant and occurs as patches with minor sphalerite in replacement of silicate or elements and in vein of comb quartz crosscutting the rock. Stibnite is late relative to arsenopyrite.

**SA11-1** shows an heterogeneous texture marked by deformed and partially recrystallized elements of hydrothermalized rhyolite with quartz and altered feldspar in a fine-grained matrix of quartz and disseminated arsenopyrite (Figure 12). The rock is crosscut by veins of quartz which occurs as coarse-grained elongated grains and comb grains with minor sulfides: tetrahedrite-tennantite mineral series, sphalerite and chalcopyrite. Quartz at the contact with sulfides is specially rich in rutile inclusions.

**SA11-2** is a highly hydrothermalized rhyolitic rock turned in a barren comb quartz vein (Figure 13). The hydrothermalized rock essentially consists of sericitic-rich rhyolitic elements, in a fine-grained elongated hydrothermal quartz, white mica and disseminated arsenopyrite.

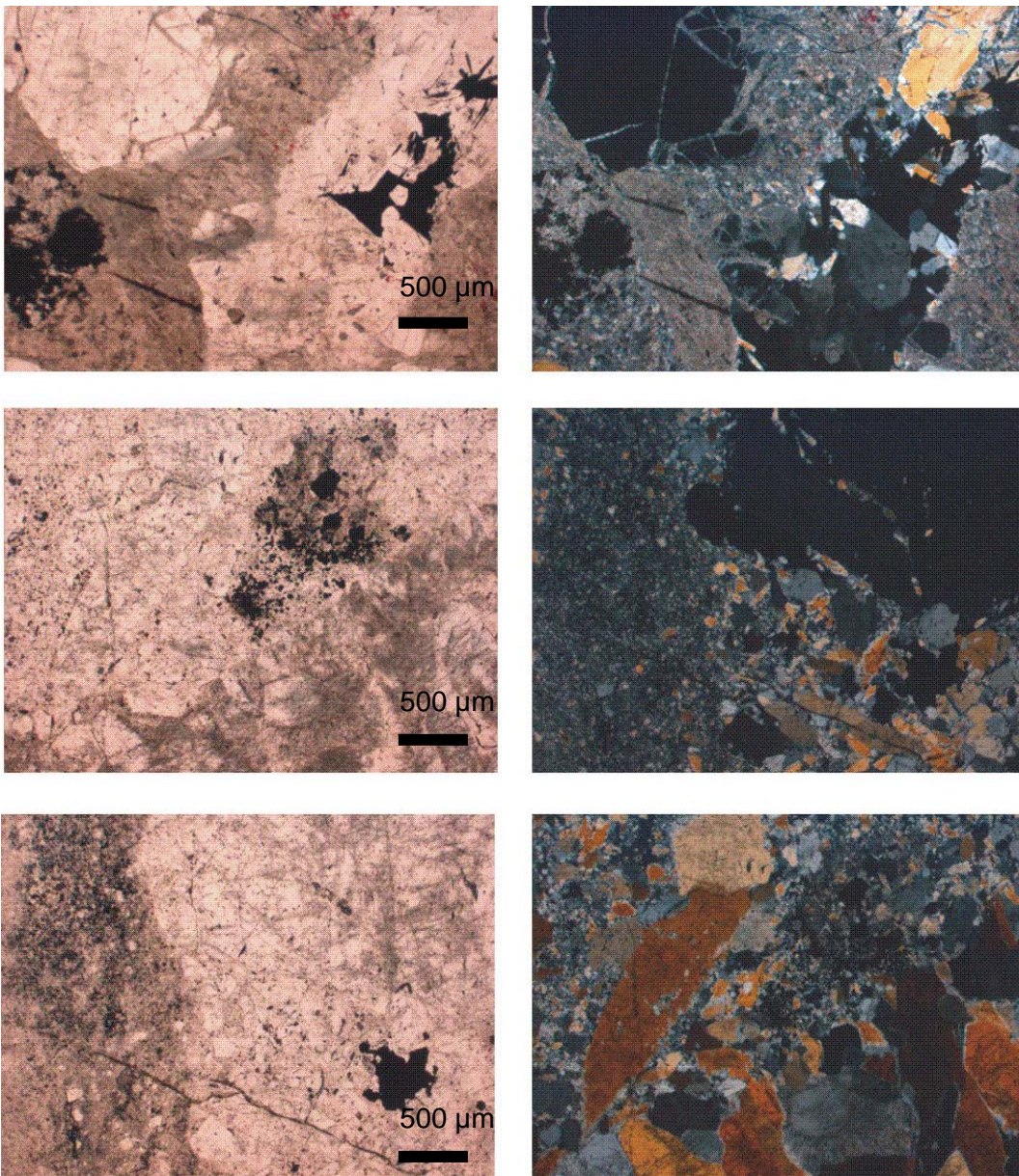


Figure 12 - micrographs of Brecca mineralization – samples SA9 and SA11-1

a	b	<p><i>a (LN), b (LP) – SA9 - Rock consisting of rhyolitic quartz in a fine-grained matrix of quartz, white mica and patches of arsenopyrite and pyrite. A vein of comb quartz and stibnite crosscut the rock. c (LN), d (LP) – SA11-1 - Element of hydrothermalized rhyolitic rock with disseminated arsenopyrite in a matrix of microcrystalline quartz, the whole crosscut by a vein of comb quartz. e (LN), f (LP) – SA11-1 - Vein of comb quartz and freibergite crosscutting hydrothermalized rhyolitic rock containing fine-grained arsenopyrite disseminated in the matrix.</i></p>
c	d	
e	f	



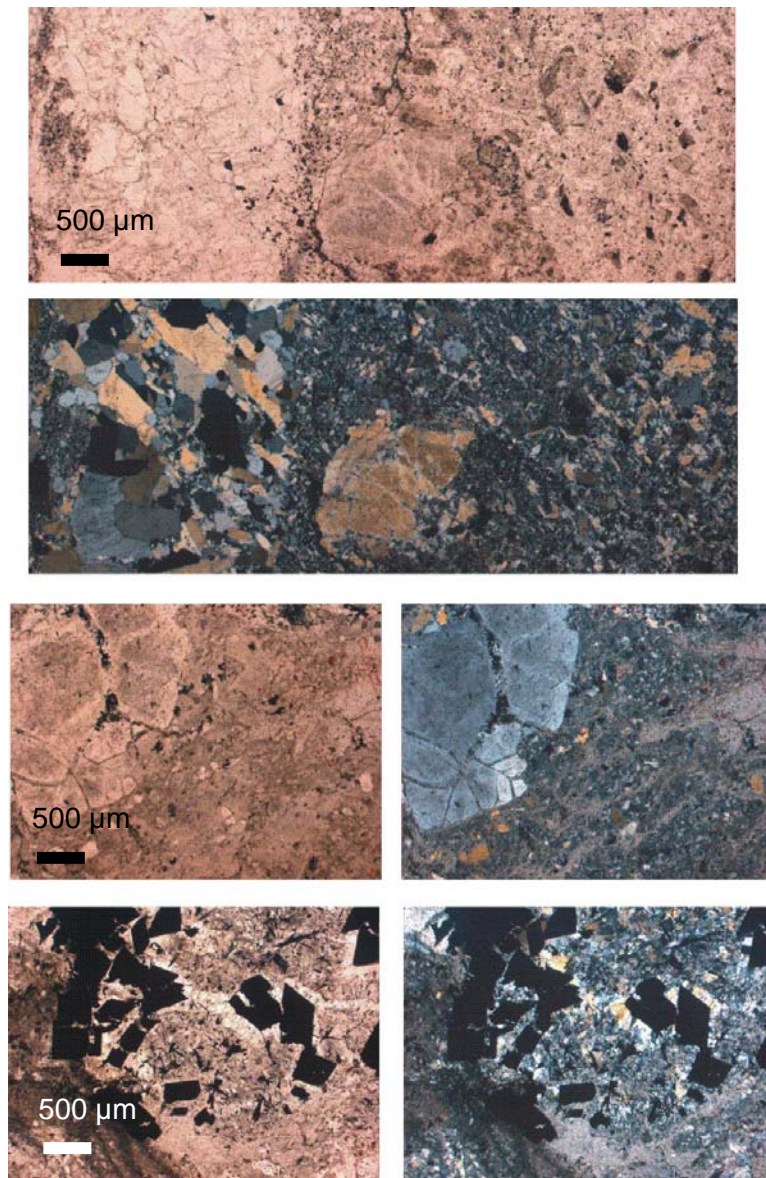


Figure 13 - micrographs of Brecca mineralization – microtextures of the samples SA11-2 and SA11-3

a	
b	
c	d
e	f

a (LN), b (LP) – SA11-2 – vein of comb quartz which crosscuts a hydrothermalized rock consisting elements of rhyolitic rock (white mica rich clasts, broken rhyolitic quartz..) in a matrix of unoriented elongated grains of quartz (“rice grain”). Comb quartz of the vein rim shows a fabric oblique to the contact. c (LN), d (LP) – SA11-3 – hydrothermalized rhyolitic rock consisting of rhyolitic quartz in a matrix of fine-grained quartz and white mica. A discrete orientation is underlined by rhyolitic quartz and white mica. e (LNA), f (LPNA) – SA11-3 – disseminated coarse-grained arsenopyrite and pyrite in the hydrothermalized rhyolitic rock. A network of very fine veinlets of quartz associated with stibnite crosscut the rock. Some of these veinlets crosscut and surround arsenopyrite grains.

**SA11-3** is a wholly hydrothermalized rhyolitic rock consisting of coarse-grained quartz and large flakes of white mica with numerous titanium oxides (original biotite?) in a matrix of microcrystalline quartz and white mica (Figure 13). Quartz grains were initially coarse, as suggested by global extinction of some populations of quartz plages (relics of rhyolitic quartz ?, early hot quartz veins ?). Fine-grained white mica infills fractures affecting coarse-grained quartz and matrix. Coarse-grained quartz and white mica underline a discrete orientation (foliation?). Sulfides are dominantly arsenopyrite, pyrite and stibnite. Arsenopyrite and pyrite with minor inclusions of pyrrhotite are coarse grained and undifferently surrounded by white mica and quartz of the matrix, and by palisadic quartz in stockwork zones. A fine quartz-stibnite stockwork overprinting the early texture. Stibnite is associated with minor sphalerite, rutile and traces of galena.

## 5.2. ANALYTICAL TECHNIQUES

Microscopic observations in transmitted and reflected light were completed by using a scanning electron microscope (SEM) equipped with a back-scattered electron (BSE) detector.

Arsenopyrite and minor associated ore minerals were analyzed with a Cameca SX 50 electron microprobe at BRGM. The used program included 13 elements with analytical settings of, acceleration voltage 20 kV, beam current 12 nA, counting time of 10 s for As, Bi, Cd, Cu, Fe, Mn, Pb, S, Sb, Zn, 20 s for Ag and Sn, 30 s for Co and Ni, 40 s for Au and a beam with a diameter of 2-5µm. Natural in-house minerals were used as standards. Limits of detection are calculated for each element, taking account analytical conditions (Table 3)

*Table 3 - detection limits of elements analyzed in arsenopyrite, taking account analytical conditions.*

Element	Ag	As	Au	Bi	Cd	Co	Cu	Fe	Mn	Ni	Pb	S	Sb	Sn	Zn
limit in ppm	647	891	398	1032	1096	274	557	547	501	270	908	188	778	480	749

## 5.3. ORE CHARACTERISATION

### 5.3.1. sample SA8

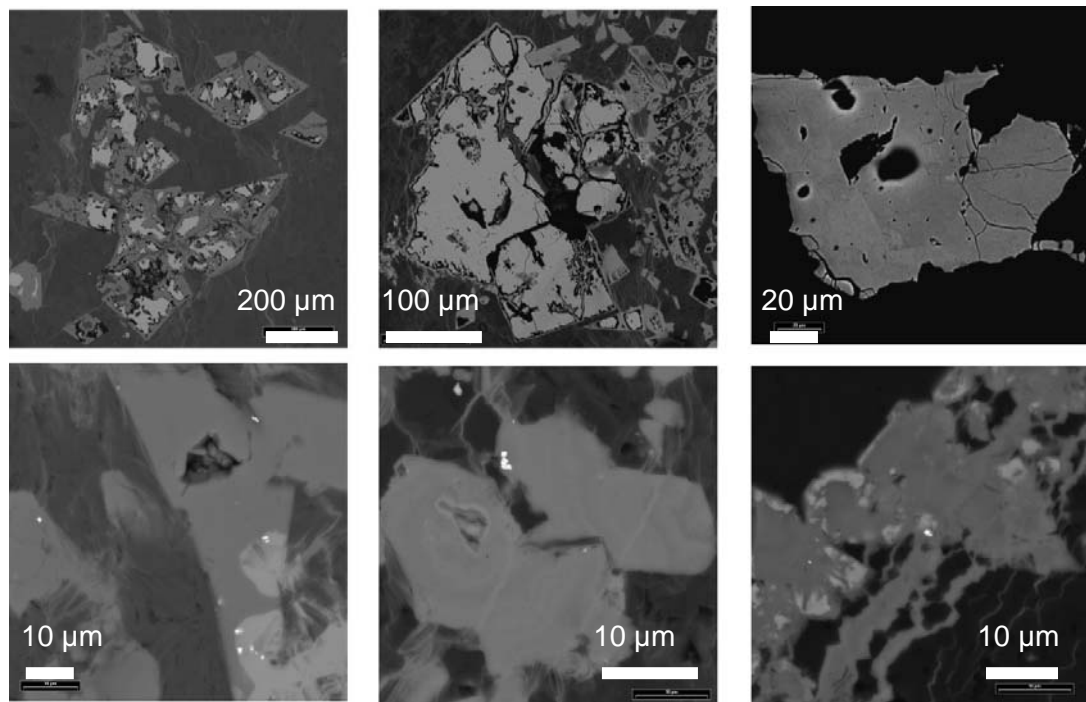
Ore consists of dominant arsenopyrite with minor pyrite. Arsenopyrite occurs as early disseminated medium-sized euhedral grains (around 200-400 µm) (Aspy I) and as fine-grained euhedral grains in veinlets (Aspy II). Pyrite occurs as disseminated 100-200 µm-sized cubic grains associated with early arsenopyrite.

Weathering largely affects ore minerals. Arsenopyrite is partially transformed in scorodite (Figure 14a). Pyrite seems to be more resistant to weathering than arsenopyrite (Figure 14b). SEM backscattered electron image of the early generation of arsenopyrite indicates a chemical zoning (Figure 14c). Jarosite was rarely observed

(Figure 14d). No gold particle was visible in unweathered arsenopyrite and specially in the first generation of arsenopyrite (Aspy I). At the opposite micronic particles of native gold are abundant in scorodite. Rare micronic gold particles were also observed in the quartz matrix. The chemical composition of preserved arsenopyrite ranges from 29 to 32 atomic percent As and 32-33 atomic percent Fe (Annexe 2). Sb content varies between 0 and 10770 ppm.

Early coarse-grained arsenopyrite shows a chemical zoning and a different chemical composition than fine-grained arsenopyrite in veinlets. Grain cores of aspy I are characterized by the lowest As content (from 28.3 to 29.8 at%), the highest Fe content around 33.2 at %, high Sb content (7720-10770 ppm) and no visible/detected gold. Grain rims are large and characterized by significantly higher As content (from 30.7 to 32.0 at %), relative constant Fe content around 33.0 at %, low Sb content and relative systematic significant gold content (one nul value and nine values between 690-2810 ppm Au).

The second generation of arsenopyrite in veinlets exhibits a larger range of As content than early arsenopyrite : between 41.1 and 44.6 at %, and high Sb contents (up to 10680 ppm) and not systematic gold content.



a	b	c
d	e	f

Figure 14 - SEM backscattered electron image of ore in sample SA8

*a* : partial alteration of arsenopyrite in scorodite ; *b* : comparative of associated pyrite ; *c* : chemical zoning of early arsenopyrite ; *d* : jarosite associated with scorodite and particles of native gold – presence of hydrothermal white mica ; *e* : total weathering of arsenopyrite in scorodite – presence of particles of native gold ; *f* : idem e with formation of secondary supergene pyrite ?

The micronic size of gold particles in partially weathered arsenopyrite makes impossible their analysis with the electron microprobe. Results are always mixing of gold with arsenopyrite. The approximate estimation of Au/Au+Ag ratio in three particles ranges between 0.92 and 1.00.

### 5.3.2. Sample SA9

Arsenopyrite occurs as disseminated 200-300 µm-sized euhedral grains. SEM backscattered electron image indicates a discrete significant zoning with a light rim which is richer in Sb and locally contains inclusions of stibnite (Figure 15 a, b). Stibnite essentially occurs as abundant disseminated grains associated with minor sphalerite and apatite containing inclusions of yttrium phosphates (Figure 15c). No gold particle was visible.

The chemical composition of arsenopyrite varies from 30.7 to 34.9 atomic percent As and atomic percent Fe of 32.3-33.4 at % (Annexe 1). Grain cores are characterized by 30.7-33.2 at % As, 32.7-33.3 at % Fe and Sb content lower than 4550 ppm. Rims are As-richer (31.2-34.7 at %), constant Fe and Sb contents up to 49860 ppm.

Even no gold particle was observed, scarce significant gold contents (from 960 to 2920 ppm) were detected by electron microprobe.

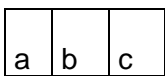
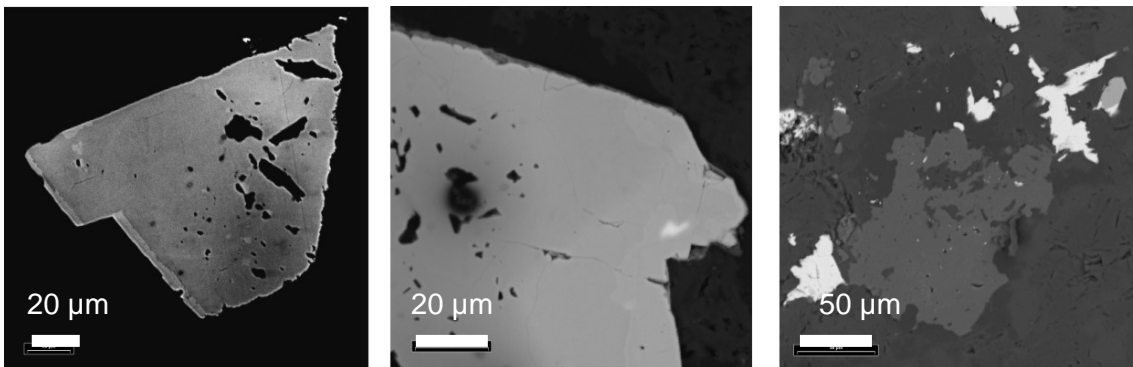


Figure 15 - SEM backscattered electron image of ore in sample SA9

*a: aspect of an arsenopyrite grain partially broken down into scorodite, and showing a small lighter and Sb- rich rim ; b : detail of a light Sb-rich rim with inclusion of stibnite ; c : characteristic assemblage of stibnite, sphalerite.*

### 5.3.3. sample 11-1

Ore essentially consists of disseminated fine-grained euhedral arsenopyrite in the hydrothermalized and brecciated rhyolite. Arsenopyrite does not show chemical zoning. A fine-grained arsenopyrite in veinlets is considered as secondary. Grey copper, sphalerite and chalcopyrite are present only in the vein of comb quartz and are very

scarce (Figure 16). SEM observations provide evidence of jamesonite associated with grey copper in the quartz vein, and also of numerous arsenopyrite micronic grains and a native gold particle in quartz of the hydrothermalized and brecciated rhyolite.

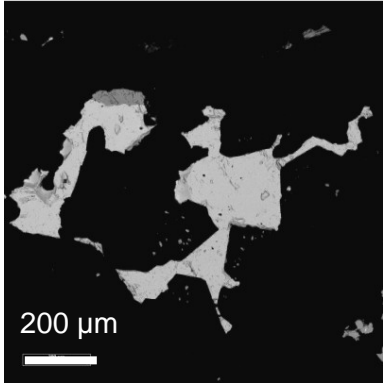


*Figure 16 - sample SA11-1 - SEM backscattered electron image of grey copper in ore*

The chemical composition of disseminated arsenopyrite varies from 29.3 to 31.5 atomic percent As, atomic percent Fe of 33.3-33.7 at % and Sb content lower than 1230 ppm (Annexe 1). There is no significant change of composition between core and rim.

Arsenopyrite II in veinlets is slightly different : 29.6-31.8 As at %, 32.1-33.1 Fe at % and Sb content between 800 and 10300 ppm. Two low values of gold content were detected in arsenopyrite.

Grey copper of the quartz vein has a freibergite composition with an Ag content of 2.7 atomic percent (Annexe 2).

#### **5.3.4. sample 11-2**

Arsenopyrite is present as disseminated fine-grained arsenopyrite. No associated sulfide was found. Arsenopyrite is automorphic and does not present any chemical zoning (Figure 17). No gold was visible.

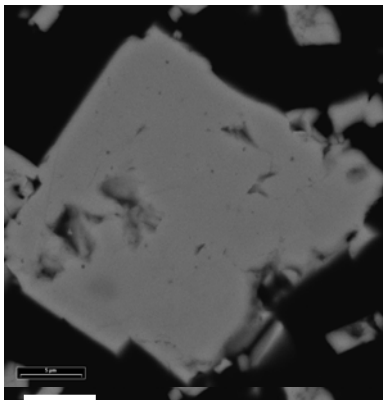


*Figure 17 - Backscattered electron image of arsenopyrite in sample 11-2.*

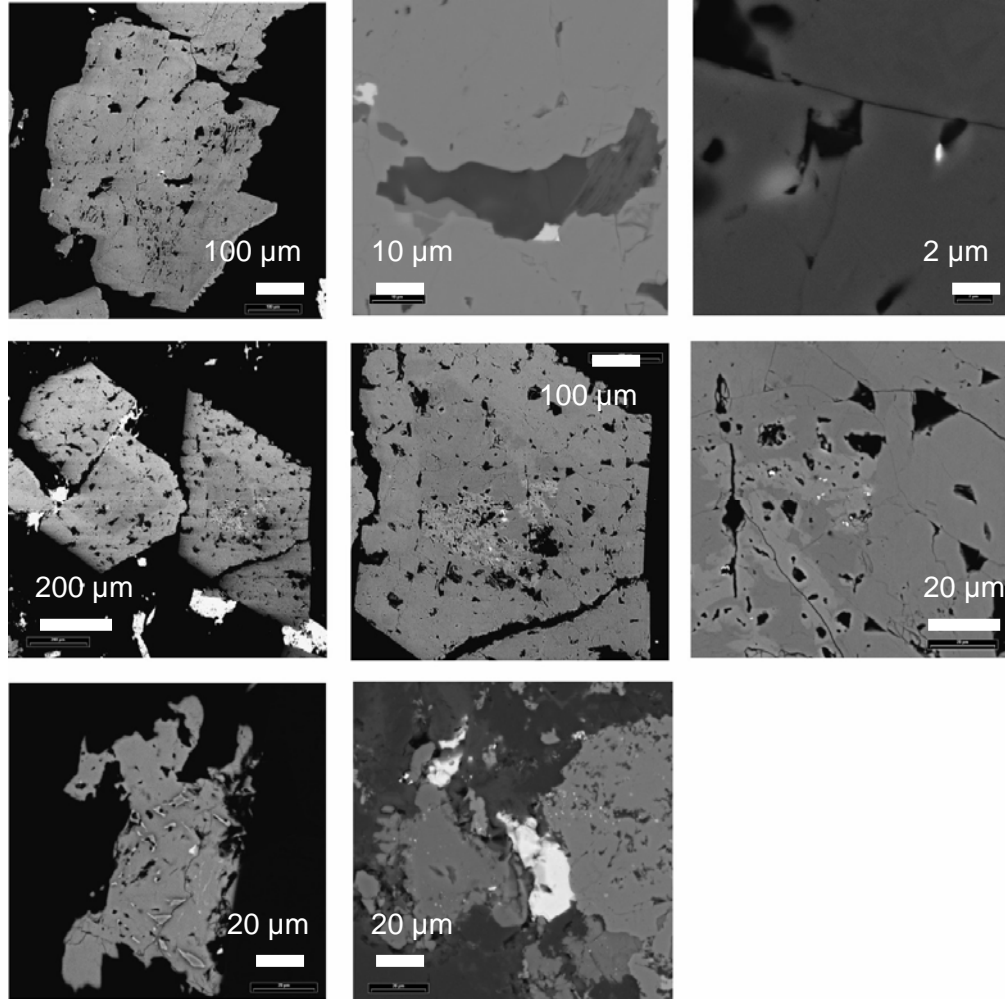
Chemical composition of arsenopyrite is quite homogeneous : 29.4-31.2 at % As and 33.3-33.7 at % Fe (Annexe 1). Scarce significant Au, Sb and Pb contents were detected.

### 5.3.5. sample 11-3

Arsenopyrite is abundant in the sample 11-3. It is coarse-grained and automorphic. Most of the grains exhibit a zoning shown by a dark core with a small Sb content and a lighter rim with a S/As ratio lighter than the core and no Sb in backscattered electron image (Figure 18 a and d ; Figure 19). No trace of gold zoning was detected with the electron microprobe (Figure 19). Most of the grains are fractured. The borders of microfractures and the very fine rims of the arsenopyrite grains are light in backscattered electron image ; they are rich in Sb and contain small grains of stibnite and jamesonite. The core of one arsenopyrite grain show an exclusive ( ?) inclusion of biotite ± chlorite + quartz + Kfeldspar + sulfides + aurostibnite (Figure 18 b). Gold is observed as micronic inclusions of native gold in core of arsenopyrite grains ( Figure 18c) but also associated with microfractures and Sb-rich zones (Fig 15e). Pyrite is rare and associated with arsenopyrite.

Stibnite occurs late crosscutting and partially replacing arsenopyrite and pyrite. Replacement of pyrite by dominant stibnite with minor galena is locally well developed (Figure 18f). SEM observations confirm that stibnite is associated with minor sphalerite, apatite and rutile but also with scarce berthierite, cobaltite, galena in inclusion in rutile and REE-rich phosphates in inclusion in apatite (Figure 18g).

Arsenopyrite shows significant chemical variations, confirming element cartography (Annexe 1). Core and rim of grains show slight different chemical compositions in As (respectively 29.8 and 30.5 at. %) and Sb (respectively 0-7680 and 0-4220 ppm ), for a constant Fe content (33.0 atomic percent). A late crystallization of arsenopyrite observed as fine rims around grains and also along microfractures crosscutting grains is characterized by a very different composition : 32.6-33.2 at. % As and Sb content up to 13690 ppm. Gold particles have a Au/Au + Ag between 0.7 and 0.9.



a	b	C
d	e	F
g	h	

Figure 18 - SEM backscattered electron image of ore in sample SA11-3

*a: aspect of arsenopyrite grain with some very discret chemical zoning and containing aurostibnite and gold inclusions ; b : detail of inclusion with quartz + feldspar + biotite/chlorite + sulfides + aurostibnite ; c : detail of gold inclusion ; d : arsenopyrite grains showing strong chemical zoning ; e, f : details of the grain core with presence of gold and stibnite inclusions – the core as the rest of the grain are strongly microfractured ; g : example of stibnite growing at the depends of early pyrite and galena ; h : micrograph of sphalerite and cobaltite.*

Sample 11-3

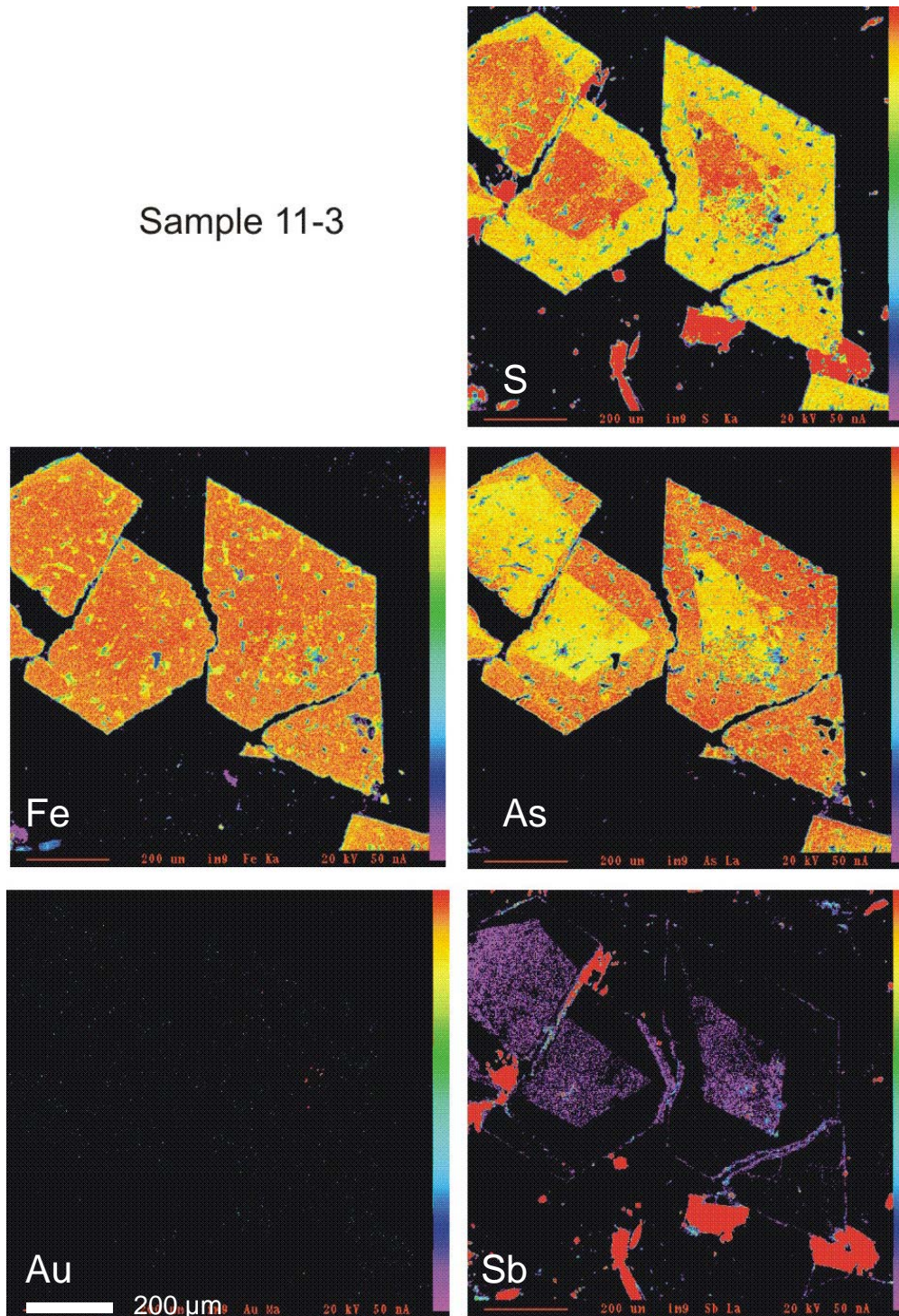


Figure 19 - Element cartography of two zoned grains of arsenopyrite – The euhedral grains of arsenopyrite show a chemical zoning with a core enriched in S and Sb and a rim enriched in As. Small inclusions of gold are observed in the core of arsenopyrite grains.



### 5.3.6. Sample SA19

Arsenopyrite exhibits a partial weathering affecting specially the cores and the fine rims of the arsenopyrite grains (Figure 20a). Gold is visible as micronic particles in weathered parts of arsenopyrite (Figure 20b, c) but never in clean grains.

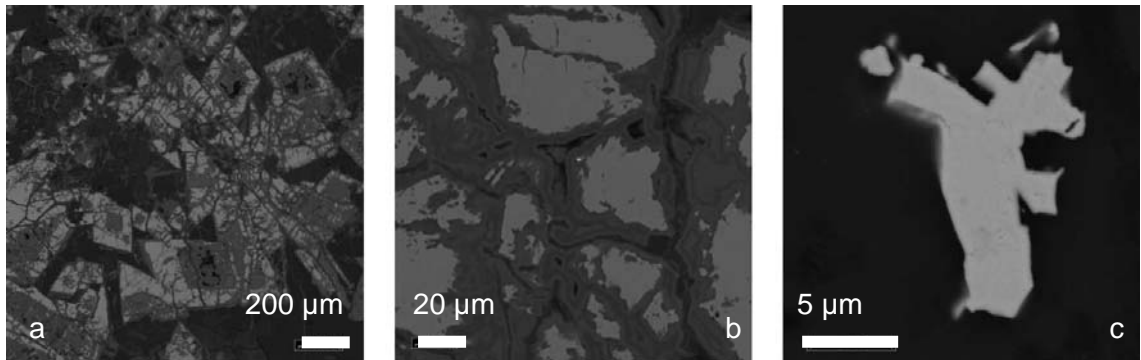


Figure 20 - micrographs of sample SA19. a. weathered arsenopyrite; b., c. particles of gold in weathered arsenopyrite

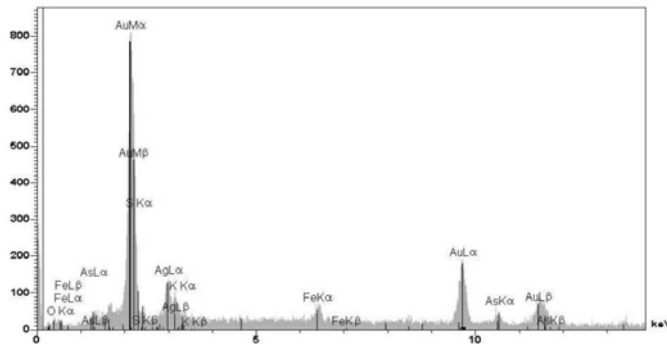
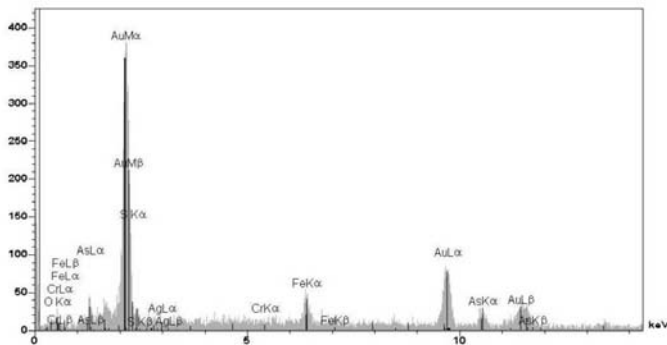


Figure 21 - EDS spectra of two gold particles. The first one is silver-bearing gold; the second one is silver-free.



Particles show different compositions : some are pure gold others contain small content of silver ( Figure 21a, b).

## 5.4. CONDITIONS OF ORE GENESIS

### 5.4.1. Paragenetic succession

The observations of the five mineralised samples provide evidence of two main stages of ore deposition (Table 44). The first stage (Fe-As-Au-Sb) is essentially represented by the deposition of disseminated arsenopyrite with minor pyrite in the quartz-white mica hydrothermalised host-rock. White mica is clearly deformed and some quartz grains are fractured with infilling of deformed white mica. Arsenopyrite occurs as zoned coarse grains in samples SA8 and SA11-3 and as medium to fine grains in other samples. Patches of stibnite in samples SA9 could be present relatively early in the system. The second stage (Sb-Pb-Zn-Ag) is characterised by the deposition of Sb-rich minerals (freibergite, stibnite, berthierite) in veins of comb quartz. Veinlets of fine-grained arsenopyrite correspond to the infilling of microfractures affecting hydrothermalised hostrock at the vicinity of quartz-Sb-rich minerals veins.

*Table 4 - description of the major stages of ore deposition observed in the five studied samples of ore from the Brecca ore deposit*

Sample	stage 1	stage 2	weathering stage
SA8	disseminated zoned coarse-grained arsenopyrite, pyrite in hydrothermalized fine-grained matrix of host-rock	veinlets of fine-grained arsenopyrite along microfractures	partial weathering of arsenopyrite - native gold only observed in scorodite resulting from the weathering of the arsenopyrite of the stage 2
SA9	disseminated medium to fine-grained arsenopyrite, stibnite patches in replacement of minerals ?	stibnite, sphalerite in veins of comb quartz	partial weathering of arsenopyrite
SA11-1	disseminated medium-to fine-grained arsenopyrite in hydrothermalized host-rock	veinlets of fine-grained totally weathered arsenopyrite along microfractures, veins of comb quartz with freibergite, sphalerite, chalcopyrite and jamesonite	
SA11-2	disseminated medium-to fine-grained arsenopyrite in hydrothermalized host-rock	veinlets of fine-grained arsenopyrite along microfractures, barren vein of comb quartz	partial weathering of arsenopyrite
SA11-3	patch of zoned coarse-grained arsenopyrite, pyrite in hydrothermalized host-rock, ? Relics of rhyolitic quartz, coarse-quartz layers?	brecciation associated with quartz-stibnite stockwork with minor sphalerite and berthierite	

### 5.4.2. Chemical composition of arsenopyrite - Gold deposition

Chemical composition of arsenopyrite varies with its facies (Table 5) and permits to detail the paragenetic succession and determine the gold deposition (Table 6).

Table 5 - Summary of the chemical variations of arsenopyrite related with its type and with its zoning

		As	Fe	S	total	As at	Fe at	S at
SA8	Aspy I core	41.97	34.85	22.01	98.82	29.78	33.18	36.50
	Aspy I rim	44.59	34.43	21.06	100.08	31.82	32.96	35.11
	Aspy II	43.07	34.22	21.81	99.09	30.69	32.70	36.29
SA9	Aspy core	43.25	34.54	21.46	99.24	30.87	33.07	35.78
	Aspy rim	44.62	33.66	20.01	98.30	32.58	32.94	34.08
SA11-1	Aspy I core	43.84	35.13	21.51	100.49	31.01	33.34	35.56
	Aspy I rim	43.50	34.64	21.60	99.74	30.94	33.05	35.90
	Aspy II	43.10	33.97	21.63	98.71	30.87	32.64	36.20
SA11-2		42.71	35.17	21.71	99.58	30.35	33.52	36.04
SA11-3	Aspy core	42.11	34.74	22.37	99.22	29.81	32.97	36.98
	Aspy rim	42.81	34.57	21.82	99.20	30.50	33.04	36.32
	Aspy core *	44.74	34.09	20.31	99.13	32.27	32.97	34.20
	Aspy fine rim	45.02	33.61	19.62	98.25	32.92	32.98	33.52

Table 6 - Description of the major stages observed in the five studied samples of ore from the Brecca ore deposit

		As-Fe-Sb-Au stage	Sb-stage
pyrrhotite	FeS	---	
pyrite	FeS <sub>2</sub>	-----	
Arsenopyrite	FeAsS		
core of coarse grains	Sb-rich As42-43	-----	
rim of coarse grains and medium to fine grains	As43-45		-----
local very fine rims of grains and microcracks in grains	Sb-rich As44-45		-- --
gold in arsenopyrite lattices		----	
veinlets	Sb-rich As43		-- - - - -
chalcopyrite	CuFeS <sub>2</sub>		-----
freibergite	(Ag, Cu, Fe) <sub>12</sub> (Sb, As) <sub>4</sub> S <sub>13</sub>		-----
jamesonite	Pb <sub>4</sub> FeSb <sub>6</sub> S <sub>14</sub>		-----
cobaltite	CoAsS		-----
stibnite	Sb <sub>2</sub> S <sub>3</sub>		-- - - - -
berthierite	FeSb <sub>2</sub> S <sub>4</sub>		-- - - - -
galena	PbS		-----
sphalerite	ZnS		-----
aurostibnite	AuSb <sub>2</sub>	----	
gold		-----	-- --

The coarse-grained arsenopyrite (samples SA8 and SA11-3) shows cores which are rich in Sb, characterised by an As content around 30 at. %. It (sample SA11-3) also contains inclusions of micronic native gold associated with aurostibnite. That provides evidence for the early presence of Au and Sb in the hydrothermal fluid. The rims of coarse-grained arsenopyrite exhibit a different composition marked by a slightly higher As content (31-32 at. %) and the lowest Sb contents. This composition is comparable to quite homogeneous composition of medium to fine-grained arsenopyrite. Significant and relatively systematic gold contents were found for this arsenopyrite composition. In unweathered grains gold is invisible (Au in lattice), whereas gold occurs as micronic particles in arsenopyrite weathered in scorodite. This second stage is the most representative of the gold ore, with the systematic presence of Au associated with arsenopyrite. Sb, even in low content in arsenopyrite is present in the fluid at this stage, as suggested by the early deposition of Sb minerals such as stibnite, jamesonite (observed in inclusions in arsenopyrite).

Late fine rims of coarse grains and of fractures crosscutting grains have quite similar composition. They show the highest As content (around 33 at. %) and high Sb content ; they are quite synchronous of the main stibnite deposition. Fine-grained arsenopyrite in veinlets of the samples SA8 and SA11-1 represents a small percentage of the ore. Its composition is quite similar in the both case. In sample SA11-1, it is similar to those of early disseminated medium to fine-grained arsenopyrite. In the sample SA8, its composition is intermediate between core and rims of early coarse-grained arsenopyrite. That strongly suggests this secondary arsenopyrite corresponds to a partial local remobilisation of early arsenopyrite during late stage of deformation and fracturation contemporaneous of emplacement of stibnite ± freibergite-quartz veins. Gold at this stage essentially occurs as numerous micronic particles of native gold in partially weathered grains of arsenopyrite. It probably represents a partial remobilisation of the gold stock present in early arsenopyrite.

### **5.4.3. Pressure-temperature conditions of ore deposition**

Crystallization temperatures of arsenopyrite were approximately estimated using the arsenopyrite geothermometer of Kretschmar and Scott (1976), based on the projection of As activity in the stability field of arsenopyrite and on the assumption that pyrite and arsenopyrite were at equilibrium.

Even a slight chemical evolution of coarse-grained arsenopyrite was observed, the As content ranging between 30 and 32 at. % indicates high formation temperatures, around 350-400°C. The observation of a preserved micronic biotite grain associated with feldspar, aurostibnite as inclusion in a core of arsenopyrite is consistent with high formation temperatures of early stage.

Despite a lack of pressure data, the textures such as fine-grained quartz followed by comb quartz associated with Sb stage strongly suggest a shallow emplacement of mineralisation (< 5 km; Dowling and Morison, 1988).

## 6. Discussion-conclusion

The Au ore of the Baccu Locci district are hosted by highly deformed and hydrothermalized rocks whose protolith seems to be a metamorphosed volcanic and sedimentary rocks. They consist of boudinaged phenocrysts of quartz and less commonly feldspar, elongated parallel to the foliation, in a matrix of sericite and a dark amorphous material. The matrix is highly deformed, with shear bands and a crenulation schistosity parallel to the main foliation observed in the field. The San Riccardo vein is located along a high angle, oblique fault, that post date the above described mylonite. Along the fault a narrow cataclastic mylonitic zone is well developed. Observation of mineralization provides evidence of two stages. The first stage is associated with boudins of coarse- to fine-grained quartz, arsenopyrite and feldspar and is synchronous with the high angle fault and related cataclasis. The second stage is represented by microcrystalline quartz veinlets with chalcopyrite and galena that cut the quartz boudins and the early arsenopyrite. These two stages could be related to the two parageneses identified in the vein (Table 2).

The Au-Sb ore of the Brecca deposit is hosted by deformed and hydrothermalized rocks consisting of elements of volcanic quartz, rare crystals of feldspar and flakes of white mica (original biotite ? attested by numerous titanium oxides associated with) in a matrix of fine-grained quartz and sericite. Relictual textures suggest that protolith is rather a rhyolitic volcanoclastic rock (crystal-bearing tuf) than a lava. Textures of microcrystalline quartz and sericite are various. Quartz can be deformed hot quartz, fine-grained xenomorphic and typical of hydrothermal quartz, unoriented elongated quartz of different sizes (rice grain texture), automorphic grains. In the hydrothermalized rocks, sericite can be disseminated in matrix or as more or less oriented anastomosed network reworking already silicified volcanoclastic rock. Preferential orientation of deformed coarse-grained quartz and locally white mica of the fine-grained matrix attests of deformation in the ductile/brittle domain during deposition of this sericite which is often related with early automorphic arsenopyrite. The paragenesis reveals the succession of an early As-Fe stage represented by disseminations of coarse-grained automorphic arsenopyrite associated with a sericite alteration and a second Sb-Cu-Pb-Zn-Ag stage represented by veinlets of comb quartz with freibergite, sphalerite, jamesonite, chalcopyrite and late stibnite. The local preferential orientation underlined by sericite seems to indicate that the As-Fe stage began quite synchronously with a ductile/brittle deformation. That is consistent with deposition temperatures around 350-400°C obtained on early arsenopyrite. The presence of rare medium-grained arsenopyrite with quite undeformed elongated quartz and veinlets of secondary arsenopyrite infilling microfractures attests that the As-Fe stage went on in the brittle domain. The second stage is late and only occurs as veins of comb quartz fracturing rock.

The most representative stock of gold is present at the first stage (Fe-As) with Sb, as attests the significant Sb content in the cores of coarse-grained arsenopyrite, the presence of rare aurostibnite inclusions associated with biotite/chlorite + K-feldspar in

arsenopyrite. Gold essentially occurs as native gold in inclusion of coarse-grained arsenopyrite and atomic gold in lattices of disseminated coarse to fine-grained arsenopyrite. It is also present in late arsenopyrite veinlets which are interpreted in our samples as local remobilization of early ore during emplacement of the Sb-rich veins and stockwork. No arsenopyrite needles were observed. In most of the cases, micronic gold is observed in weathered arsenopyrite, that suggests a possible change of state of gold related to weathering.

Both the paragenetic successions observed at San Riccardo and at Brecca show two stages : a first arsenopyrite-pyrite stage associated with a sericitic alteration and a second stage represented by vein infilling with quartz and Sb-Au-Pb-Zn-Ag mineralization. A mineralization with two stages is a characteristic of most of the gold deposits of the SE Sardinia (Garbarino et al., 2003) and of main Variscan gold mineralization in French Massif Central (Bouchot et al., 2005). The San Riccardo deposit, with free gold, shows a paragenetic and structural evolution similar to the "deep-seated " gold deposits as defined in the French Massif Central (Bouchot et al., 2005). In contrast, the presence of Au in the lattices of arsenopyrite and of aurostibnite at the first stage and quartz texture (rice grain, comb quartz) are only observed, in the French Massif Central in the shallow gold deposits such as the Au-(Sb) La Marche district (Bouchot et al., 1994, 2005).

## 7. Bibliography

Allibone A., McCuaig T.C., Harris D., Etheridge M., Munroe S., Byrne D., Amanor J., Gyapong W., 2002. Structural controls on gold mineralization at the Ashanti Deposit, Obuasi, Ghana. *Economic Geology and the Bulletin of the Society of Economic Geologists*, vol. 9, pp. 65-93

Bakos F., Carcangiu G., Fadda S., Mazzella A., Valera R., 1991. The gold mineralization of Baccu Locci (Sardinia, Italy): origin, evolution and concentration processes. *Terra Nova*, 2, 232-237.

Bouchot V., Gros Y., Bonnemaïson M., 1990. Structural control of the auriferous shear zone of the Saint-Yrieix District, Massif central, France: evidence from the Le Bourneix and Laurières gold deposits. *Econ. Geol.*, 54, 1315-1327.

Bouchot V., Gros Y., Piantone P., 1994. Dynamics of shallow late-Variscan gold mineralization; the Le Châtelet Au-arsenopyrite quartz veins, Massif Central, France. *Mineralium Deposita* 29 (6), 461-473

Bouchot V., Ledru P., Lerouge C., Lescuyer J.L., Milesi J.P. 2005. Late-Variscan mineralising systems related to orogenic processes: the French Massif Central. *Ore Geology Reviews, Volume 27, Issues 1-4, November 2005, Pages 169-197.*

Carmignani L., Conti P., Barca S., Cerbai N., Eltrudis A., Funedda, A., Oggiano G., Patta E.D., 2001. Note illustrative della Carta Geologica d'Italia alla scala 1: 50.000 – Foglio 549-Muravera. Progetto CARG Sardegna L.R. 305/89–Servizio Geologico d'Italia-Regione Autonoma della Sardegna, pp.140.

Carmignani L., Oggiano G., Barca S., Conti P., Salvadori I., Eltrudis A., Funedda A., Pasci S., 2000. Geologia della Sardegna- Note illustrative della Carta Geologica della Sardegna alla scala 1: 200.000. *Mem.Descr. della Carta Geol. d'It.*, Vol. LX, pp.283.

Conti P., Funedda A., Cerbai N. 1998. Mylonite development in the Hercynian basement of Sardinia (Italy). *Journal of Structural Geology*, Vol. 20, No. 2/3, pp. 121 to 133.

Dowling K., Morrison G.W., 1988. Application of quartz textures to the classification of North Queensland gold deposits. *Abstracts - Geological Society of Australia* 22, 272-276.

Funedda A., Naitza S., Tocco S., 2005. Caratteri giacimentologici e controlli strutturali nelle mineralizzazioni idrotermali tardo-erciniche ad As-Sb-W-Au del basamento metamorfico paleozoico della Sardegna Sud-orientale. *Res. Ass. Min. Sarda*, a. CX, n. 1., Iglesias, 25-46.

Garbarino C., Naitza S., Tocco S., Farci A., Reyner J., 2003. Orogenic gold in the Paleozoic basement of SE Sardinia (Italy). In: Eliopoulos et al. (eds.) "Mineral Exploration and sustainable development", Millpress, Rotterdam, 767-770 .

Kretschmar, U., Scott, S.D., 1976. Phase relations involving arsenopyrite in the system Fe-As-S and their application. *Canadian Mineralogist* 14, 364-386.

Schneider, H.J. (1972): Schichtgebundene NE-metall- und F-Ba Lagerstätten im Sarrabus-Gerrei Gebiet, SE Sardinien. I. Bericht: zur Lagerstaettenkunde und Geologie. *N. Jb. Miner. Mh.* 12: 529.

Zucchetti, S.C., 1958. The lead-arsenic sulfide ore deposit of Baccu Locci (Sardinia, Italy). *Econ. Geol.*, 53: 867-876.



## **Appendices**

Annexe 1 - Whole-rock geochemical data of the Spilloncargiu and San Riccardo ore deposits

Annexe 2 – EPMA analyses of arsenopyrite from the Brecca Au-Sb ore deposit

Annexe 3 – EPMA analyses of tetrahedrite from the Brecca Au-Sb ore deposit



## Annexe 1

Preliminary whole-rock geochemical data on the Spilloncargiu and San Riccardo ores, are reported in the two tables below.

*Whole-rock geochemistry (ICP-MS analyses; samples from different mineworks, a set of selected trace elements, ppm unit) of the Su Spilloncargiu stratabound mineralisation. F1: oxidation/cementation zone, Santa Teresa adit; F10 primary sulfide ore, Santa Barbara adit.*

Sample	Au	Ag	Zn	Pb	Cu	As	Se	Bi	Sb	W	Sn	Mo	V	Cr	Ni
F1	54	637	>10000	>10000	>10000	6500	420	816	170	n.d.	5	25	127	110	28.4
F10	32	75	>10000	>10000	9180	628	113	0.5	24	n.d.	2	8	55	295	18.6

*Whole-rock geochemistry (ICP-MS analyses, for a set of selected trace elements, ppm unit) from two different traverses performed in the San Riccardo veins. SA4-10: Southern traverse; SA16-19 Northern traverse.*

sample	Au	Ag	Zn	Pb	Cu	As	Se	Bi	Sb	W	Sn	Mo	V	Cr	Ni
SA4	1890	248	464	>10000	924	65000	n.d.	0.5	1300	n.d.	6	5	157	88	2.4
SA5	4240	230	186	>10000	537	100000	n.d.	17.5	390	n.d.	1	n.d.	3	202	5.5
SA6	2610	200	32	>10000	225	52000	n.d.	4.5	140	n.d.	4	n.d.	57	142	7.3
SA7	286	61	38	>10000	259	22000	n.d.	4.2	160	n.d.	2	2	71	189	5.3
SA8	5260	170	11	>10000	797	47000	n.d.	1.6	130	n.d.	2	n.d.	n.d.	93	5.4
SA9	99	n.d.	127	409	77	8000	n.d.	0.9	12	15	4	n.d.	119	147	12
SA10	77	58	27	>10000	931	2160	n.d.	1.3	56	26	7	n.d.	67	131	12.4
SA11	4490	280	275	>10000	2540	140000	n.d.	16.3	500	n.d.	5	n.d.	4	255	11.2
SA16	1600	197	2690	>10000	2260	81000	n.d.	38	85	n.d.	1	n.d.	38	170	11.2
SA17	2830	127	34	>10000	612	100000	n.d.	4	140	n.d.	n.d.	n.d.	6	272	16.7
SA18	3570	84	10	>10000	149	120000	n.d.	17.8	414	n.d.	n.d.	n.d.	1	221	8.6
SA19	749	57	3600	6480	244	22000	n.d.	0.4	62	n.d.	0.2	5	156	147	13.5



## Annexe 2

## Ponctual EPMA analyses of arsenopyrite in samples SA8, SA9, SA11-1, SA11-2, SA11-3

Point			As	Fe	S	total	As at	Fe at	S at	Ag	Au	Bi	Pb	Sb
5	SA8	Aspy I core	41.95	34.83	22.14	100.07	29.74	33.13	36.68	590	-	1280	1650	7720
6	SA8	Aspy I core	40.34	35.35	22.96	100.22	28.35	33.33	37.70	750	-	1250	2280	10770
7	SA8	Aspy I core	41.36	35.16	22.79	100.82	29.00	33.07	37.34	1340	0	2020	1590	10050
52	SA8	Aspy I core	41.97	34.85	22.01	98.82	29.78	33.18	36.50	-	-	-	1230	9530
2	SA8	Aspy I rim	43.48	34.93	21.43	99.95	30.95	33.37	35.65	0	0	-	-	0
3	SA8	Aspy I rim	44.69	34.50	20.79	100.33	31.99	33.14	34.77	610	2810	0	0	-
4	SA8	Aspy I rim	44.62	34.33	20.74	99.96	32.04	33.07	34.79	0	1650	0	0	1110
9	SA8	Aspy I rim	43.96	34.59	21.14	100.32	31.38	33.13	35.26	0	1350	1270	2320	-
11	SA8	Aspy I rim	44.17	34.18	20.97	99.71	31.72	32.93	35.19	0	920	-	1000	650
53	SA8	Aspy I rim	43.23	34.49	21.57	99.29	30.83	33.01	35.95	-	820	-	-	3310
54	SA8	Aspy I rim	43.07	34.46	21.70	99.24	30.75	33.00	36.20	-	690	-	-	-
55	SA8	Aspy I rim	44.33	33.65	21.08	99.05	31.91	32.49	35.45	-	1560	-	1090	-
56	SA8	Aspy I rim	44.19	34.56	21.23	99.98	31.48	33.03	35.33	-	990	-	1650	-
57	SA8	Aspy I rim	44.59	34.43	21.06	100.08	31.82	32.96	35.11	-	790	-	1110	0
41	SA8	Aspy II	44.63	33.48	21.21	99.32	32.05	32.26	35.60	-	980	0	950	-
42	SA8	Aspy II	43.36	33.68	22.03	99.07	30.89	32.19	36.68	-	770	0	-	4740
50	SA8	Aspy II	42.38	33.90	22.09	98.37	30.24	32.46	36.84	-	0	1130	-	8530
51	SA8	Aspy II	41.14	34.69	22.87	98.70	28.99	32.79	37.66	-	0	1480	1320	10680
13	SA8	Aspy II	42.89	34.45	22.16	100.44	30.33	32.69	36.63	0	-	1310	1480	6000
14	SA8	Aspy II	42.72	34.85	21.45	100.20	30.47	33.35	35.75	1100	0	2390	2790	5520
17	SA8	Aspy II	44.37	34.48	20.83	99.87	31.82	33.18	34.91	0	-	0	-	-
22	SA9	Aspy core	43.38	33.81	20.77	98.64	31.53	32.97	35.27	-	-	-	3570	2250
23	SA9	Aspy core	44.60	32.71	19.37	97.43	33.23	32.70	33.72	630	0	0	1480	4550
26	SA9	Aspy core	44.20	34.26	20.61	99.27	31.93	33.21	34.79	0	-	1000	0	550
27	SA9	Aspy core	44.70	34.65	20.68	100.38	32.01	33.29	34.61	0	-	1050	2030	-
28	SA9	Aspy core	44.47	34.61	20.97	100.50	31.74	33.14	34.97	510	0	1300	1790	870
33	SA9	Aspy core	43.81	34.15	21.22	99.63	31.42	32.86	35.55	1190	-	-	1690	580
34	SA9	Aspy core *	43.26	33.08	20.06	96.89	32.10	32.93	34.78	-	1160	0	1370	1860
35	SA9	Aspy core	43.11	34.57	21.77	99.64	30.69	33.02	36.22	-	760	0	0	840
42	SA9	Aspy core	43.14	34.60	21.17	99.34	30.97	33.32	35.52	0	0	-	0	3760
18	SA9	Aspy rim	44.52	34.77	20.68	100.09	31.91	33.43	34.63	-	0	1270	0	0
19	SA9	Aspy rim	44.48	34.42	20.85	99.95	31.89	33.10	34.92	480	-	0	-	0
20	SA9	Aspy rim	44.70	34.68	20.94	100.44	31.88	33.18	34.90	0	0	0	0	1180
24	SA9	Aspy rim	45.69	33.54	19.06	99.11	33.67	33.16	32.83	0	0	1810	0	6280
25	SA9	Aspy rim	45.72	33.05	19.67	99.17	33.50	32.49	33.68	10	0	0	0	7100
30	SA9	Aspy rim	44.73	34.32	20.84	100.60	32.01	32.94	34.84	730	2920	960	1990	-
31	SA9	Aspy rim	44.04	34.17	20.85	99.14	31.77	33.06	35.14	540	0	-	0	0
32	SA9	Aspy rim	44.24	34.29	20.92	99.95	31.75	33.01	35.07	-	0	1550	2230	830
36	SA9	Aspy rim	43.18	34.06	20.96	98.90	31.24	33.05	35.44	0	990	3160	0	2090
37	SA9	Aspy rim	46.34	32.06	18.01	98.38	34.93	32.42	31.73	-	-	0	-	18100
38	SA9	Aspy rim	43.89	30.43	16.46	96.27	34.69	32.26	30.40	830	0	0	3250	49860
39	SA9	Aspy rim	44.08	33.81	20.53	98.53	32.07	32.99	34.88	0	0	0	-	640
43	SA9	Aspy rim	44.47	34.06	20.39	99.14	32.25	33.14	34.55	0	670	-	1330	0

Variscan gold mineralisation of Baccu Locci and Brecca, southeastern Sardinia

Point		As	Fe	S	total	As at	Fe at	S at	Ag	Au	Bi	Pb	Sb	
1	SA11-1	42.54	35.41	22.06	100.01	29.98	33.48	36.32	0	0	0	-	4730	
2	SA11-1	42.42	35.46	22.46	100.34	29.73	33.35	36.78	-	0	0	0	2950	
3	SA11-1	43.55	35.07	21.70	100.31	30.80	33.27	35.86	0	0	0	-	-	
4	SA11-1	43.60	35.15	21.38	100.14	30.96	33.49	35.48	0	-	-	-	-	
5	SA11-1	41.78	35.48	22.66	99.92	29.30	33.38	37.14	0	0	-	1540	2780	
6	SA11-1	42.12	35.30	22.56	99.98	29.60	33.28	37.04	0	0	0	-	1680	
7	SA11-1	43.45	35.23	21.57	100.26	30.77	33.48	35.69	0	0	1170	-	-	
14	SA11-1	43.76	34.72	21.46	99.94	31.09	33.09	35.63	700	-	-	980	2180	
16	SA11-1	42.71	35.35	21.60	99.66	30.26	33.60	35.76	-	0	1440	-	5880	
17	SA11-1	42.45	35.59	21.89	99.93	29.91	33.64	36.05	0	-	-	-	8670	
18	SA11-1	44.09	34.74	21.11	99.94	31.45	33.23	35.18	-	0	1070	-	1160	
19	SA11-1	42.71	34.42	21.45	98.58	30.60	33.08	35.92	1200	630	0	-	6950	
22	SA11-1	43.80	35.25	21.36	100.41	31.03	33.50	35.36	-	0	-	-	-	
23	SA11-1	43.83	34.99	21.07	99.89	31.28	33.50	35.13	0	0	0	-	-	
24	SA11-1	43.95	34.77	21.14	99.85	31.38	33.30	35.26	-	450	-	-	-	
25	SA11-1	44.19	35.13	20.78	100.09	31.55	33.65	34.67	790	0	-	1010	-	
26	SA11-1	43.08	35.40	21.79	100.27	30.44	33.56	35.97	0	0	-	-	-	
27	SA11-1	43.94	34.75	20.78	99.47	31.54	33.47	34.85	-	0	-	-	-	
28	SA11-1	43.17	35.09	21.36	99.62	30.78	33.56	35.59	-	0	-	1560	0	
30	SA11-1	43.85	35.35	21.00	100.20	31.20	33.74	34.91	0	0	1380	1730	-	
31	SA11-1	43.94	35.46	21.13	100.53	31.16	33.74	35.01	-	0	0	1170	0	
52	SA11-1	Aspy I core	43.96	35.30	21.78	101.43	30.87	33.25	35.73	0	-	0	2200	1230
55	SA11-1	Aspy I core	43.73	34.96	21.25	100.01	31.16	33.42	35.38	0	-	0	0	0
			43.84	35.13	21.51	100.72 #	31.01	33.34	35.56					
53	SA11-1	Aspy I rim	43.51	34.27	21.52	99.62	31.08	32.84	35.92	680	-	950	0	-
54	SA11-1	Aspy I rim	43.48	35.01	21.69	100.36	30.79	33.26	35.88	0	0	0	-	1120
44	SA11-1	Aspy II	43.01	33.18	21.60	98.68	31.05	32.14	36.43	500	0	1060	-	6380
45	SA11-1	Aspy II	44.43	34.00	21.24	99.77	31.80	32.65	35.52	0	-	0	0	800
46	SA11-1	Aspy II	43.07	34.91	22.28	100.91	30.26	32.91	36.57	-	0	-	-	5440
47	SA11-1	Aspy II	41.65	34.34	22.38	99.62	29.60	32.74	37.16	0	0	-	1360	10300
48	SA11-1	Aspy II	44.04	33.53	21.03	99.27	31.78	32.46	35.47	0	0	-	0	6490
49	SA11-1	Aspy II	43.16	34.02	20.90	98.24	31.34	33.14	35.45	-	0	0	0	1440
50	SA11-1	Aspy II	42.36	33.81	22.01	99.42	30.29	32.43	36.78	-	0	-	1430	10160
32	SA11-2		42.13	35.50	21.98	99.61	29.82	33.70	36.34	-	0	0	3020	
33	SA11-2		41.66	35.49	22.40	99.55	29.40	33.60	36.94	0	1540	1070	0	
34	SA11-2		42.93	35.28	21.37	99.57	30.59	33.72	35.58	710	-	0	1130	
35	SA11-2		42.56	35.05	21.88	99.48	30.23	33.41	36.32	0	-	0	-	
36	SA11-2		43.43	34.89	21.11	99.43	31.08	33.49	35.29	0	1210	1060	-	
43	SA11-2		42.90	35.43	21.61	99.93	30.41	33.70	35.79	0	1160	1530	-	
44	SA11-2		42.51	34.90	21.81	99.22	30.25	33.31	36.26	0	-	1560	3180	
45	SA11-2		42.61	35.31	21.95	99.88	30.15	33.52	36.29	0	0	-	-	
48	SA11-2		43.63	34.67	21.25	99.55	31.21	33.27	35.51	0	-	0	-	

## Variscan gold mineralisation of Bacchu Locci and Brecca, southeastern Sardinia

Point		As	Fe	S	total	As at	Fe at	S at	Ag	Au	Bi	Pb	Sb
11	SA11-3 Aspy rim	43.95	34.40	21.37	99.72	31.37	32.94	35.63	-	0	-	-	-
13	SA11-3 Aspy rim	43.41	34.22	21.54	99.17	31.07	32.85	36.01	-	0	0	950	-
31	SA11-3 Aspy rim	42.37	34.68	21.92	98.97	30.18	33.14	36.49	0	400	0	-	3560
32	SA11-3 Aspy rim	41.49	34.99	22.45	98.93	29.39	33.25	37.15	0	10	0	-	4220
7	SA11-3 Aspy core *	42.90	34.56	21.82	99.27	30.45	32.90	36.18	0	0	-	2220	9070
8	SA11-3 Aspy core *	45.75	33.94	19.59	99.28	33.16	33.00	33.17	0	0	-	-	12540
9	SA11-3 Aspy core *	45.56	33.77	19.53	98.85	33.19	33.00	33.24	0	0	-	1380	11640
10	SA11-3 Aspy core	44.27	34.72	21.20	100.20	31.52	33.17	35.27	0	0	-	-	0
14	SA11-3 Aspy core	41.99	34.62	22.22	98.83	29.86	33.02	36.92	-	0	0	-	2950
15	SA11-3 Aspy core	40.69	34.80	23.30	98.79	28.59	32.81	38.25	-	0	0	1020	6280
16	SA11-3 Aspy core	40.58	34.92	23.31	98.81	28.51	32.91	38.26	-	-	0	940	6380
17	SA11-3 Aspy core	41.07	35.00	23.28	99.34	28.73	32.84	38.05	-	0	-	-	7680
28	SA11-3 Aspy core	44.06	34.36	20.94	99.36	31.65	33.10	35.14	0	0	0	0	950
33	SA11-3 Aspy fine rim	45.24	33.56	19.64	98.45	33.02	32.86	33.50	-	0	0	0	11300
34	SA11-3 Aspy fine rim	45.31	33.74	19.43	98.48	33.19	33.15	33.25	0	0	-	-	8120
35	SA11-3 Aspy fine rim	44.50	33.54	19.78	97.82	32.56	32.93	33.82	0	0	0	0	13690
54	SA11-3	43.95	34.80	21.08	99.83	31.38	33.32	35.16	-	0	-	-	880
55	SA11-3	43.27	35.15	21.35	99.77	30.82	33.59	35.53	0	0	-	-	0
56	SA11-3	43.47	34.99	21.05	99.51	31.04	33.51	35.12	1030	0	0	1960	3290
57	SA11-3	42.65	35.31	21.28	99.24	30.49	33.86	35.55	0	-	1310	0	1330
58	SA11-3	44.07	34.97	21.17	100.21	31.34	33.37	35.18	1060	-	-	0	0
59	SA11-3	42.93	35.22	21.36	99.51	30.61	33.69	35.59	720	0	-	0	900
60	SA11-3	43.37	34.65	20.96	98.98	31.20	33.44	35.23	0	-	-	1960	-





**Annexe 3***Ponctual EPMA chemical analyses of tetrahedrite in the sample SA11-1*

	11-1	11-1	11-1
<b>Cu</b>	34.75	34.67	34.74
<b>S</b>	24.13	24.24	24.40
<b>Fe</b>	5.18	5.11	5.30
<b>Sb</b>	27.20	27.31	26.94
<b>As</b>	2.10	2.31	2.35
<b>Zn</b>	1.40	1.29	1.42
<b>Au</b>	0.00	0.00	0.00
<b>Mn</b>	0.03	0.00	0.00
<b>Sn</b>	0.10	0.12	0.05
<b>Bi</b>	0.00	0.01	0.11
<b>Ag</b>	4.91	4.94	5.17
<b>Pb</b>	0.03	0.16	0.00
<b>Cd</b>	0.00	0.00	0.03
<b>TOTAL</b>	99.83	100.15	100.51
<b>Cu cat</b>	31.95	31.81	31.68
<b>S cat</b>	43.96	44.06	44.09
<b>Fe cat</b>	5.41	5.34	5.50
<b>Sb cat</b>	13.05	13.08	12.82
<b>As cat</b>	1.64	1.80	1.81
<b>Zn cat</b>	1.26	1.15	1.26
<b>Au cat</b>	0.00	0.00	0.00
<b>Mn cat</b>	0.03	0.00	0.00
<b>Sn cat</b>	0.05	0.06	0.02
<b>Bi cat</b>	0.00	0.00	0.03
<b>Ag cat</b>	2.66	2.67	2.78
<b>Pb cat</b>	0.01	0.05	0.00
<b>Cd cat</b>	0.00	0.00	0.02





**Scientific and Technical Centre**  
3, avenue Claude-Guillemain - BP 36009  
45060 Orléans Cedex 2 – France – Tel.: +33 (0)2 38 64 34 34